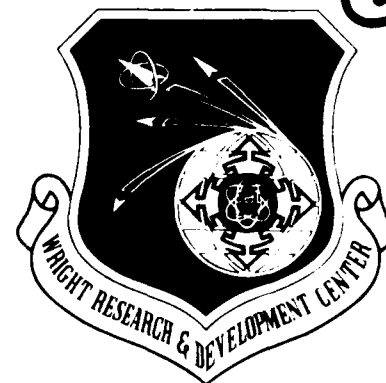


DTIC FILE COPY

2

WRDC-TR-90-2058

AD-A225 372



**GROUND ENVIRONMENT CHARACTERIZATION
OF STOVL FIGHTER PROPULSION SYSTEMS**

Randolph W. Spratt

Universal Technology Corporation
Signal Hill TechnCenter
4031 Colonel Glenn Highway
Dayton, Ohio 45431-1600

August 1990

Final Report for Period November 1988 - November 1989

Approved for public release; distribution is unlimited.



AERO PROPULSION AND POWER LABORATORY
WRIGHT RESEARCH DEVELOPMENT CENTER
AIR FORCE SYSTEMS COMMAND
WRIGHT-PATTERSON AIR FORCE BASE OH 45433-6563

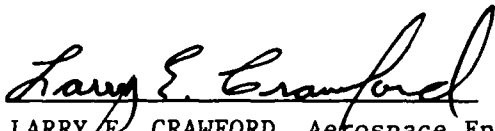
90 08 14 121

NOTICE

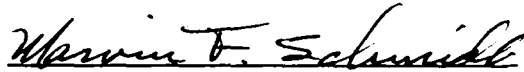
When Government drawings, specifications, or other data are used for any purpose other than in connection with a definitely Government-related procurement, the United States Government incurs no responsibility or any obligation whatsoever. The fact that the government may have formulated or in any way supplied the said drawings, specification, or other data, is not to be regarded by implication, or otherwise in any manner construed, as licensing the holder, or any other person or corporation; or as conveying any rights or permission to manufacture, use, or sell any patented invention that may in any way be related thereto.

THIS REPORT HAS BEEN REVIEWED BY THE OFFICE OF PUBLIC AFFAIRS (ASD/PA) AND IS RELEASABLE TO THE NATIONAL TECHNICAL INFORMATION SERVICE (NTIS). AT NTIS IT WILL BE AVAILABLE TO THE GENERAL PUBLIC INCLUDING FOREIGN NATIONS.

THIS TECHNICAL REPORT HAS BEEN REVIEWED AND IS APPROVED FOR PUBLICATION.

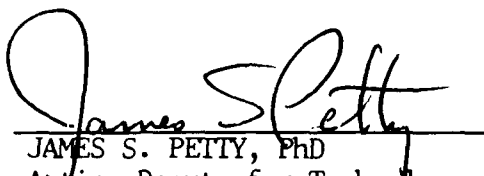


LARRY E. CRAWFORD, Aerospace Engineer
Engine Integration & Assessment Branch



MARVIN F. SCHMIDT, Chief
Engine Integration & Assessment Branch

FOR THE COMMANDER



JAMES S. PETTY, PhD
Acting Deputy for Technology
Turbine Engine Division
Aero Propulsion & Power Laboratory

If your address has changed, if you wish to be removed from our mailing list, or if the addressee is no longer employed by your organization, please notify WRDC/POTA, WPAFB, OH 45433-6563 to help us maintain a current mailing list.

Copies of this report should not be returned unless return is required by security considerations, contractual obligations, or notice on a specific document.

REPORT DOCUMENTATION PAGE				Form Approved OMB No. 0704-0188		
1a. REPORT SECURITY CLASSIFICATION UNCLASSIFIED			1b. RESTRICTIVE MARKINGS			
2a. SECURITY CLASSIFICATION AUTHORITY			3. DISTRIBUTION/AVAILABILITY OF REPORT Approved for public release; Distribution is unlimited.			
2b. DECLASSIFICATION/DOWNGRADING SCHEDULE						
4. PERFORMING ORGANIZATION REPORT NUMBER(S)			5. MONITORING ORGANIZATION REPORT NUMBER(S) WRDC/TR-90-2058			
6a. NAME OF PERFORMING ORGANIZATION Universal Technology Corporation (UTC)		6b. OFFICE SYMBOL (If applicable)	7a. NAME OF MONITORING ORGANIZATION Wright Research and Development Center Aero Propulsion and Power Laboratory			
6c. ADDRESS (City, State, and ZIP Code) 4031 Colonel Glenn Highway Dayton, Ohio 45431-1600			7b. ADDRESS (City, State, and ZIP Code) Wright-Patterson AFB, Ohio 45433-6563			
8a. NAME OF FUNDING/SPONSORING ORGANIZATION		8b. OFFICE SYMBOL (If applicable)	9. PROCUREMENT INSTRUMENT IDENTIFICATION NUMBER F33615-88-C-2823			
8c. ADDRESS (City, State, and ZIP Code)			10. SOURCE OF FUNDING NUMBERS			
			PROGRAM ELEMENT NO. 62203F	PROJECT NO. 3066	TASK NO. 11	WORK UNIT ACCESSION NO. 68
11. TITLE (Include Security Classification) Ground Environment Characterization of STOVL Fighter Propulsion Systems						
12. PERSONAL AUTHOR(S) Randolph W. Spratt						
13a. TYPE OF REPORT Final		13b. TIME COVERED FROM 88/11 TO 89/11		14. DATE OF REPORT (Year, Month, Day) 1990, August		
15. PAGE COUNT 86						
16. SUPPLEMENTARY NOTATION						
17. COSATI CODES			18. SUBJECT TERMS (Continue on reverse if necessary and identify by block number)			
FIELD	GROUP	SUB-GROUP	STOVL, Ground Environment, Landing Pad Response			
19. ABSTRACT (Continue on reverse if necessary and identify by block number)						
<p>The report contains information on the ground environment produced by STOVL propulsion systems. Data on impingement flow fields, heat transfer rates of impinging jets, and STOVL fighter exhaust characteristics are included. An analysis method was developed by UTC to estimate STOVL ground environments. Ground environments were estimated for the AV-8, Remote Augmented Lift (RAL), Remote Exhaust (REX), Hybrid Fan Vectored Thrust (HFVT), ejector augmentor, and lift plus lift/cruise propulsion systems. The effect of these ground environments on aluminum plates, asphalt concrete, Portland Cement Concrete (PCC), and steel plates was estimated. Facilities capable of conducting ground environment tests were identified. Recommendations for future ground environment study efforts are presented in the report.</p>						
20. DISTRIBUTION/AVAILABILITY OF ABSTRACT <input checked="" type="checkbox"/> UNCLASSIFIED/UNLIMITED <input type="checkbox"/> SAME AS RPT. <input type="checkbox"/> DTIC USERS			21. ABSTRACT SECURITY CLASSIFICATION UNCLASSIFIED			
22a. NAME OF RESPONSIBLE INDIVIDUAL Larry E. Crawford			22b. TELEPHONE (Include Area Code) (513) 255-2121		22c. OFFICE SYMBOL WRDC/POTA	

FOREWARD

The author wishes to acknowledge Dr. Wilber Hankey for the technical assistance he provided to this project. Dr. Hankey's work was the key to the ground environment analysis method developed for this study.

Accession For	
NTIS GRA&I	<input checked="checked" type="checkbox"/>
DTIC TAB	<input type="checkbox"/>
Unannounced	<input type="checkbox"/>
Justification	
By	
Distribution/	
Availability Codes	
Dist	Avail Codes
A-1	Special



LIST OF CONTENTS

SECTION	PAGE
1.0 INTRODUCTION	1
1.1 Objectives.	1
1.2 Approach.	1
1.2.1 Landing Pad Materials.	1
1.2.2 Ground Environment Analysis.	2
1.2.3 Test Facilities.	2
1.3 Limitations	2
1.4 Report Overview	2
2.0 LANDING PAD MATERIALS.	3
2.1 Materials Investigated.	3
2.1.1 Asphalt Concrete	3
2.1.2 Portland Cement Concrete (PCC)	4
2.1.3 Steel Decking.	4
2.1.4 Aluminum Pads.	4
2.2 Material Thermal and Mechanical Properties.	4
2.3 Material Failure Modes.	5
2.3.1 Asphalt Concrete Failure Modes	6
2.3.2 PCC Failure Modes.	6
2.3.3 Steel Decking Failure Modes.	7
2.3.4 Aluminum Pad Failure Modes	8
2.4 Estimated Material Environmental Limits	8
3.0 PROPULSION CONCEPTS STUDIED	8
3.1 Propulsion System Descriptions.	9
3.1.1 AV-8 Vectored Thrust System	9
3.1.2 REX Concept.	10
3.1.3 RAL Concept.	10
3.1.4 Ejector Augmentor Concept.	11
3.1.5 HFVT Concept	12
3.1.6 Lift Plus Lift/Cruise Concept.	12
3.2 Exhaust Characteristics of STOVL Propulsion Systems	13
4.0 GROUND ENVIRONMENT ANALYSIS.	14
4.1 Ground Environment Analysis Methodology	15
4.1.1 Flow Field Characteristics	15
4.1.2 Aerodynamic Loads.	19
4.1.2.1 Ground Plane Total Pressure	20
4.1.2.2 Ground Plane Dynamic Pressure	21
4.1.2.3 Ground Plane Shear Stress	22
4.1.2.4 Jet Induced Lift.	23
4.1.3 Thermal Loads.	24
4.1.3.1 Convection Heat Transfer.	24
4.1.3.2 Radiation Heat Transfer	27
4.1.3.3 Conduction Heat Transfer.	33
4.1.3.4 Thermal Stress.	35

LIST OF CONTENTS CONTINUED

SECTION		PAGE
4.1.4	Load Assessment.	39
4.1.4.1	Aerodynamic Loads	39
4.1.4.2	Thermal Loads	39
4.2	Propulsion Concept Ground Environment Ratings . . .	40
4.2.1	Propulsion Concept Aerodynamic Loads	40
4.2.2	Propulsion Concept Thermal Loads	41
4.2.3	Propulsion Concept Ranking	42
5.0	GROUND ENVIRONMENT TEST FACILITIES	44
5.1	Preliminary Test Facility Requirements.	44
5.2	Identified Test Facilities.	45
5.3	Test Facilities Suggested for Future Research . . .	48
6.0	CONCLUSIONS.	50
7.0	RECOMMENDATIONS.	52
	REFERENCES.	53
APPENDICES		
A.	Material Temperature Profiles	56
B.	Test Facilities	69

LIST OF FIGURES

FIGURE		PAGE
1.	Temperature Effects on PCC	6
2.	PCC Strength Reduction vs. Temperature Exposure.	7
3.	AV-8 Vectored Thrust Propulsion System	9
4.	Remote Exhaust Propulsion Concept.	10
5.	Remote Augmented Lift Propulsion Concept	11
6.	Ejector Augmentor Propulsion Concept	11
7.	Hybrid Fan Vectored Thrust Propulsion Concept.	12
8.	Lift Plus Lift/Cruise Propulsion Concept	13
9.	Jet Characteristics NPR < 1.89 - Subsonic Flow	16
10.	Jet Characteristics 2.1 < NPR < 3.85 - Moderately Under-Expanded Flow	16
11.	Jet Characteristics NPR > 3.85 - Highly Under-Expanded Flow.	17
12.	Exhaust Jet Impingement Flow Field	18
13.	Supersonic Jet Impingement Flow Field.	18
14.	Jet Impingement Flow Field for Forward Moving Aircraft	19
15.	Axisymmetric Nozzle Ground Plane Total Pressure Curve.	20
16.	Ground Plane Dynamic Pressure.	22
17.	Ground Plane Shear Stress.	23
18.	Convection Heat Transfer Rate	27
19.	Water Vapor Emissivity at One Atmosphere	30
20.	Water Vapor Pressure Correction Factor	30
21.	Carbon Dioxide Emissivity at One Atmosphere.	31
22.	Carbon Dioxide Pressure Correction Factor.	32
23.	Mixture Correction Factor.	32
24.	Radiation Heat Transfer (H/D=6).	33
25.	Temperature Profiles in PCC - 30 Btu/ft ² -sec	35
26.	Thermal Stress in Aluminum	37
27.	Thermal Stress in Asphalt Concrete	37
28.	Thermal Stress in PCC.	38
29.	Thermal Stress in Steel.	38
A-1.	Temperature Profile in Aluminum (10 Btu/ft ² -sec)	57
A-2.	Temperature Profile in Aluminum (20 Btu/ft ² -sec)	57
A-3.	Temperature Profile in Aluminum (30 Btu/ft ² -sec)	58
A-4.	Temperature Profile in Aluminum (40 Btu/ft ² -sec)	58
A-5.	Temperature Profile in Aluminum (50 Btu/ft ² -sec)	59
A-6.	Temperature Profile in Aluminum (60 Btu/ft ² -sec)	59
A-7.	Temperature Profile in Asphalt (10 Btu/ft ² -sec)	60
A-8.	Temperature Profile in Asphalt (20 Btu/ft ² -sec)	60
A-9.	Temperature Profile in Asphalt (30 Btu/ft ² -sec)	61
A-10.	Temperature Profile in Asphalt (40 Btu/ft ² -sec)	61
A-11.	Temperature Profile in Asphalt (50 Btu/ft ² -sec)	62
A-12.	Temperature Profile in Asphalt (60 Btu/ft ² -sec)	62
A-13.	Temperature Profile in PCC (10 Btu/ft ² -sec).	63
A-14.	Temperature Profile in PCC (20 Btu/ft ² -sec).	63
A-15.	Temperature Profile in PCC (30 Btu/ft ² -sec).	64
A-16.	Temperature Profile in PCC (40 Btu/ft ² -sec).	64
A-17.	Temperature Profile in PCC (50 Btu/ft ² -sec).	65
A-18.	Temperature Profile in PCC (60 Btu/ft ² -sec).	65
A-19.	Temperature Profile in Steel (10 Btu/ft ² -sec).	66

LIST OF FIGURES CONTINUED

FIGURE	PAGE
A-20. Temperature Profile in Steel (20 Btu/ft ² -sec)	66
A-21. Temperature Profile in Steel (30 Btu/ft ² -sec)	67
A-22. Temperature Profile in Steel (40 Btu/ft ² -sec)	67
A-23. Temperature Profile in Steel (50 Btu/ft ² -sec)	68
A-24. Temperature Profile in Steel (60 Btu/ft ² -sec)	68
B-1. NASA Ames Outdoor Aerodynamic Research Facility.	70
B-2. Moveable Ground Erosion Rig.	70
B-3. Shoeburyness Test Site	71
B-4. NASA Ames 80 X 120 Wind Tunnel	71
B-5. NASA Ames 40 X 80 Wind Tunnel.	72
B-6. British Aircraft Corporation 5.5 Meter Wind Tunnel	72
B-7. NASA Langley 30 X 60 Wind Tunnel	73
B-8. Boeing Cold Air Rig.	73
B-9. Boeing V/STOVL Wind Tunnel	74
B-10. British Aerospace Hot Gas Ingestion Facility	74
B-11. German/Dutch Low Speed Wind Tunnel DWN	75
B-12. McDonnell Aircraft Jet Interaction Test Apparatus.	75
B-13. Pennsylvania State University Laboratory	76
B-14. Sandia Laboratory.	76

LIST OF TABLES

TABLE	PAGE
1. Landing Pad Material Properties.	5
2. Estimated Environmental Limits	8
3. STOVL Propulsion Exhaust Characteristics	14
4. Propulsion System Pressure Estimates	40
5. Propulsion System Heat Transfer Estimates.	41
6. Residence Time Limits.	42
7. Propulsion Concept Ranking	43
8. Preliminary Test Facility Requirements	44
9. Full-Scale Test Facilities	45
10. Sub-Scale Test Facilities.	47
11. Test Parameters.	51

SUMMARY

The ground environmental characterization of Short Takeoff and Vertical Landing (STOVL) fighter propulsion systems was performed by Universal Technology Corporation (UTC) under contract with the Turbine Engine Division, Aero Propulsion and Power Laboratory of the Wright Research and Development Center (WRDC).

The objectives of the study were to identify environmental limits for landing pad materials, estimate the STOVL fighter ground environments and the effect these environments have on typical landing pads, and identify test facilities that could potentially be used for future ground environment test programs.

A literature search was conducted to find documentation on past ground environment research programs. Information was gathered on landing pad material properties, STOVL fighter propulsion system exhaust characteristics, jet impingement flow fields and ground environment analysis methods.

Preliminary environmental limits were established for aluminum, asphalt concrete, Portland Cement Concrete (PCC) and steel. The estimated environmental limits covered normal pressures, dynamic pressures and surface temperatures.

Six STOVL propulsion concepts were investigated in this study. Exhaust characteristics were estimated for AV-8 vectored thrust, ejector augmentor, Hybrid Fan Vectored Thrust (HFVT), lift plus lift/cruise, Remote Augmented Lift (RAL), and Remote Exhaust (REX) propulsion systems. Values for nozzle pressure

ratio, exhaust gas temperature and ratio of aircraft altitude to nozzle diameter (H/D) are included in the report.

An analysis method was developed to provide preliminary estimates of the ground environment loads produced by STOVL propulsion systems. The analysis includes calculations to assess the impact of aircraft ground environments on aluminum, asphalt concrete, PCC and steel landing pads. Normal pressure loads, dynamic pressure loads, shear stresses, induced lifting forces, convection heat transfer, radiation heat transfer, conduction heat transfer, material temperature profiles, residence times and thermal stresses are discussed in the analysis method.

The analysis method was used to predict ground environments for the six propulsion systems identified in the report and estimate the effect these environments have on the baseline landing pad materials. Normal pressure loads and dynamic pressure loads were calculated to be too small to damage the baseline landing pad material under normal conditions but if the landing pad contains broken and loose pieces of pavement, these pieces may be lifted and blown by the jet exhaust. The jet exhaust heat load was calculated by adding the convection and radiation heat transfer estimates together. Convection was determined to have a greater impact on the total heat transfer rate than radiation. The radiation heat transfer estimate included hot gas radiation but did not estimate the radiation emitted by hot engine parts. A conduction analysis was used to predict temperature profiles in landing pad materials. These profiles were used to estimate residence times and thermal

stresses. The thermal stress calculation used in this study unsatisfactorily predicted landing pad failure points, therefore, surface temperature was selected as the parameter to determine the point of failure. Based on the surface temperature limits, residence time limits were estimated for the landing pad materials. The residence time limits indicated that rolling landings would be needed on asphalt concrete and PCC. Rolling landings may also be necessary on aluminum and steel if a RAL system is selected or if repetitive vertical operations are conducted with the other propulsion concepts. The propulsion systems were ranked according to the severity of the heating loads. The AV-8 vectored thrust system was determined to have the least severe environment while the RAL system was calculated to possess the most severe environment.

Potential STOVL ground environment test facilities are identified in the report. Preliminary test facility capability requirements were identified. These requirements were established from an assessment of the data that should be collected in a STOVL ground environment test program. Test facilities possessing the capabilities that best matched the identified facility requirements were suggested for future test programs. The Warton Hot Gas Laboratory Ground Erosion Rig, NASA Lewis 9 X 15 wind tunnel, the Rolls Royce RB108 rig and the NASA Ames 80 x 120 low speed wind tunnel were identified for future test programs. The Warton rig and the NASA Lewis wind tunnel can be used to conduct sub-scale testing while the Rolls-Royce rig and the NASA Ames wind tunnel can conduct tests at the

full scale level. The Warton and Rolls-Royce rig may not be available for a U.S. testing program but similar facilities could set up in the U.S. Some full scale testing will be required up front to determine the split between full scale and scale model test programs.

Based on the analyses and assessments conducted in this study, two recommendations were made for future STOVL fighter ground environment research program.

- o Testing should be conducted to assess the environmental loads associated with STOVL propulsion systems and the effect these loads have on typical landing pads. The parameters that should be varied in the test program include nozzle pressure ratio, exhaust gas temperature, nozzle diameter, nozzle geometry, H/D ratio, aircraft sink rate and aircraft forward velocity.
- o An analysis method should be constructed to accurately predict the ground environments of various STOVL propulsion systems. The analysis should include a procedure to forecast landing pad life characteristics.

1.0 INTRODUCTION

The WRDC Aero Propulsion and Power Laboratory tasked UTC to investigate STOVL aircraft ground environments and their effect on landing-pad materials. The Laboratory is interested in these ground environments since propulsion system designs will be influenced by the jet/ground interaction. The study objectives, approach, assumptions and limitations are summarized in sections 1.1 through 1.3. An overview of the report is provided in section 1.4.

1.1 Objectives

The three primary objectives for this study are listed below:

1. Identify environmental limits for selected landing pad materials,
2. Investigate the ground environments associated with selected STOVL propulsion concepts to determine the effect these environments have on baseline landing pad materials, and
3. Identify test facilities best suited for future ground environment research.

1.2 Approach

An approach was developed for each of the main objectives. The step-by-step approaches used to accomplish the objectives are listed below:

1.2.1 Landing Pad Materials

1. Identify the landing pad materials to be investigated.
2. Identify the thermal and mechanical properties of the landing pad materials.
3. Identify failure modes of landing pad materials exposed to propulsion exhaust gases.
4. Review the landing pad material failure modes to determine the environmental limits for each material.

1.2.2 Ground Environment Analysis

1. Identify the STOVL propulsion concepts to be evaluated.
2. For each concept, identify the propulsion system characteristics that affect the ground environment.
3. Identify an analysis method that can determine propulsion system ground environments and the effects these ground environments have on landing pads materials.
4. Use the analysis method to determine the effect of the selected propulsion systems on the baseline landing pad materials.

1.2.3 Test Facilities

1. Document the test facility capabilities required to conduct ground environment tests.
2. Identify test facilities that can be used for ground environment tests and the capabilities of each facility.
3. Determine which facilities best meet future test requirements.

1.3 Limitations

1. The literature was limited to the DTIC information system, Wright State University library, and WRDC technical library.
2. No significant data was directly obtained from airframe or engine contractors. All contractor data was obtained from past reports.
3. The study was limited to investigating the ground environments produced by RAL, REX, HFVT, AV-8, ejector augmentor and lift plus lift/cruise STOVL propulsion systems.
4. The study was limited to determining the effects of ground environments on steel, aluminum, asphalt concrete, and PCC landing pad materials.

1.4 Report Overview

The remaining sections of the report state the findings, conclusions and recommendations made in this study. The findings

are broken down into three main sections. Information on landing pad material characteristics and limits is presented in section 2.0. STOVL propulsion exhaust characteristics are described in section 3.0 while ground environment analysis procedures and ground environment ratings are given in section 4.0. Preliminary test requirements, test facility capabilities and test facilities suggested for future research efforts are given in section 5.0. The conclusions reached in this study are presented in section 6.0. Recommendations for future ground environment research efforts are summarized in section 7.0.

2.0 LANDING PAD MATERIALS

Four landing pad materials were investigated in this study. Basic descriptions of these materials are included in section 2.1. Section 2.2 lists the thermal and mechanical properties of the landing pad materials. Landing pad failure modes associated with jet blasts are discussed in section 2.3. Estimated material environmental limits are given in section 2.4.

2.1 Materials Investigated

Asphalt concrete, PCC, steel decking and aluminum materials were investigated in the study. General descriptions of the four landing pad types are provided in sections 2.1.1 through 2.1.4.

2.1.1 Asphalt Concrete

Asphalt concrete is constructed from asphalt cement and aggregates. Asphalt cements are primarily derived from petroleum. Aggregates include gravel, sand and rock dust. The composition of these aggregates varies with location since they

are obtained from quarries near the landing pad. Asphalt cement binds the aggregates together to form asphalt concrete.

2.1.2 Portland Cement Concrete (PCC)

Portland cement binds aggregates together to form PCC. Portland cements are derived from calcined rock and clay materials. Aggregates include gravel, sand and rock dust. The composition of the cement and the aggregates varies with location since the materials are obtained from local sources. PCC is normally laid in slabs to control landing pad cracking. Joints in between the slabs are usually filled with asphalt joint filler.

2.1.3 Steel Decking

Ship decks are commonly constructed with low carbon steels and low alloy steels. Only low carbon steel decks were investigated in this study. Small ships with landing pads have decks 9/16-inch thick and aircraft carriers can have up to 2-inch thick decks. Decks are typically coated with a non-skid paint. Ship deck paint was ignored in this study.

2.1.4 Aluminum Pads

Aluminum could be used to increase the heat transfer rate of a ship deck in order to lower the deck surface temperatures. The aluminum would need to be thick or actively cooled to provide acceptable metal temperatures.

2.2 Material Thermal and Mechanical Properties

Properties of the landing pad materials were used to determine the response of the landing pad to jet exhaust. Conductivity, diffusivity, emissivity, thermal expansion

coefficient, modulus of elasticity, allowable compression load, and allowable shear load are shown for each landing pad material in table 1.

Table 1. Landing Pad Material Properties

	Aluminum	Asphalt Concrete	PCC	Carbon Steel
Conductivity ^a (Btu/sec-ft-°F)	0.038	0.000192	0.00028	0.0061
Diffusivity ^a (ft ² /sec)	0.000947	0.0000058	0.0000093	0.000129
Emissivity	0.2 ^a	0.9 ^b	0.9 ^b	0.55 ^a
Thermal Expansion Coefficient (1/°F)	0.00013 ^c	0.000005 ^d	0.000006 ^c	0.000065 ^c
Modulus of Elasticity (kpsi)	10,000 ^c	1,000 ^d	5,000 ^c	29,000 ^c
Allowable Compression Load (psi)	35,000 ^c	600 ^d	2,250 ^c	60,000 ^c
Allowable Shear Load (psi)	20,000 ^c	300 ^d	86 ^c	36,000 ^c

a Purdue University, 1970²⁹

b Incropera, 1981¹⁶

c Popov, 1972²⁸

d Heavy Trucks: Climate and Pavement Damage, 1988¹⁴

2.3 Material Failure Modes

Landing pad failure modes associated with jet blasts are identified for each landing pad material and are discussed in sections 2.3.1 through 2.3.4.

2.3.1 Asphalt Concrete Failure Modes

Melting of the asphalt cement is the predominant failure mode associated with asphalt concrete. The hot jet exhaust causes asphalt cement to flow in the temperature range of 200-350°F.¹ The melting temperature varies since the composition of the asphalt cement is variable.

The jet blast can produce a lifting force on the landing pad. If the landing pad has cracked and broken sections, these sections may be lifted and blown out of place. Temperature cycling may affect the strength and elasticity of asphalt concrete but quantitative data was not found on this phenomenon.

2.3.2 PCC Failure Modes

PCC exposed to high temperature goes through various phases of degradation. Temperature effects on PCC are shown in figure 1.

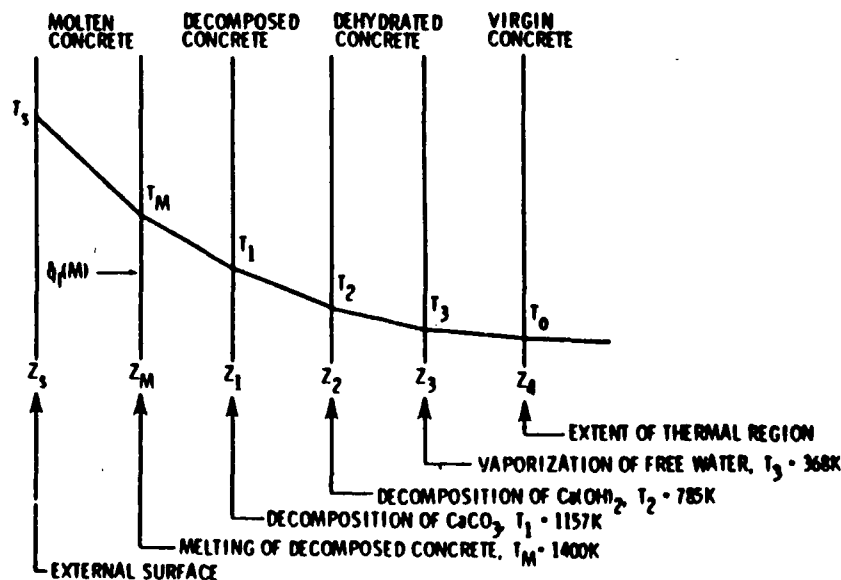


Figure 1. Temperatures Effects on PCC²⁶

High temperature exposure can induce mechanical failures in PCC such as cracking and spalling. Material strength can be

lowered when high temperature is applied to PCC. A relationship between temperature exposure and residual strength is shown in figure 2.

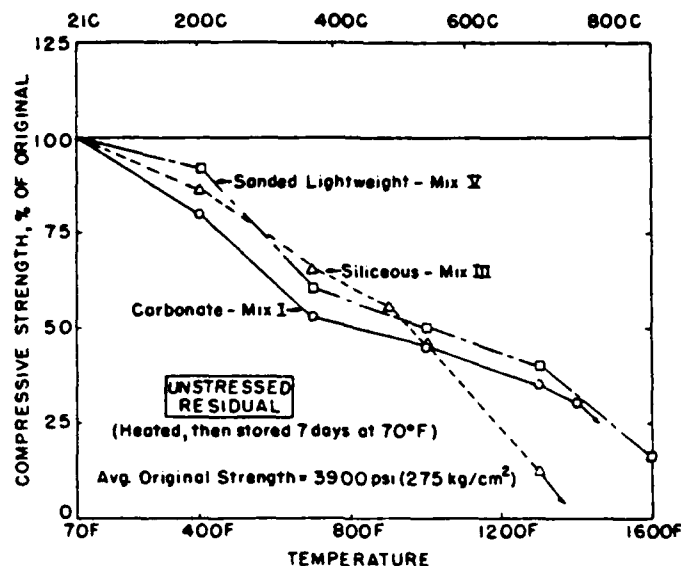


Figure 2. PCC Strength Reduction vs. Temperature Exposure²

Heat induced spalling and cracking are most likely due to thermal incompatibilities produced between the Portland cement and the aggregates. Spalling may also be caused by water vapor entrapment near the surface of PCC pavements.³³ Temperature cycling may affect PCC but no quantitative data was found on this phenomenon.

2.3.3 Steel Decking Failure Modes

The strength of low carbon steel decreases as the material temperature increases. The maximum recommended temperature for low carbon steel is 700°F.³⁴ Steel expands as the material temperature increases which may cause the deck to buckle.

2.3.4 Aluminum Pad Failure Modes

The strength of aluminum decreases as the material temperature increases. The maximum recommended temperature for aluminum is 400°F.³⁴

2.4 Estimated Material Environmental Limits

Based on the assessment conducted in the study, environmental limits were estimated for asphalt concrete, PCC, steel decking and aluminum. The estimated limits are shown in table 2.

Table 2. Estimated Environmental Limits

Landing Pad Material	Normal Pressure load limit (psi)	Dynamic Pressure limit (psi)	Temperature limit (°F)
Asphalt Concrete	600 ^a	300 ^a	200 ^c
PCC	5,000 ^b	100 ^b	600 ^d
Steel	60,000 ^b	36,000 ^b	700 ^e
Aluminum	35,000 ^b	20,000 ^b	400 ^e

a Heavy Trucks; Climate and Pavement, 1988¹⁴

b Popov, 1972²⁸

c Abraham, 1962¹

d Smith, 1978³³

e United Technologies, 1981³⁴

These limits are preliminary estimates and will need to be re-evaluated as further information is gathered on landing pad materials.

3.0 PROPULSION CONCEPTS STUDIED

The ground environments associated with six propulsion concepts were investigated in this study. These concepts were

developed for single engine fighter aircraft. Brief descriptions of the propulsion concepts are provided in section 3.1. Exhaust characteristics associated with the STOVL propulsion systems are summarized in section 3.2.

3.1 Propulsion System Descriptions

AV-8 vectored thrust, REX, RAL, ejector augmentor, HFVT and lift plus lift/cruise propulsion concepts were investigated in this study. Short summaries of each concept follow.

3.1.1 AV-8 Vectored Thrust System

The AV-8 is the only VTOL fighter aircraft operated by the US Armed Forces. Horizontal and vertical thrust is provided through four exhaust nozzles. The two front nozzles are supplied with fan air and the two rear nozzles are supplied with turbine exhaust air. The nozzles are rotated to change the thrust direction from horizontal to vertical. The engine does not have an augmentor. The AV-8 vectored thrust engine is shown in figure 3.

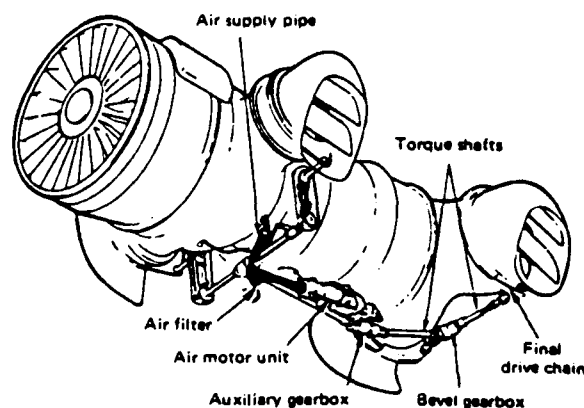


Figure 3. AV-8 Vectored Thrust Propulsion System²⁴

3.1.2 REX Concept

In a REX propulsion system, vertical lift is provided by two remotely located REX nozzles and a ventral nozzle. The REX nozzles are fed with turbine exhaust gas. During vertical operations the cruise nozzle is closed and valves open to supply turbine air to the REX nozzle air ducts. The ventral nozzle is located on the tailpipe to provide trim thrust for vertical flight operations. Thrust can be augmented in horizontal flight but not in vertical flight. A schematic of the REX concept is shown in figure 4.

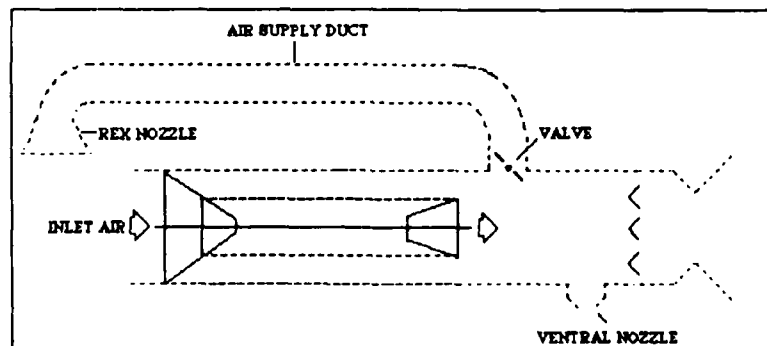


Figure 4. Remote Exhaust Propulsion Concept

3.1.3 RAL Concept

In the RAL propulsion concept, vertical thrust components are derived from two RAL nozzles and a vectoring cruise nozzle. The vectoring cruise nozzle is augmented and directed down during vertical operations. The two RAL nozzles are supplied with fan air during vertical flight operations. Burners are used to augment the fan air supplied to the RAL nozzles. The RAL propulsion concept is shown in figure 5.

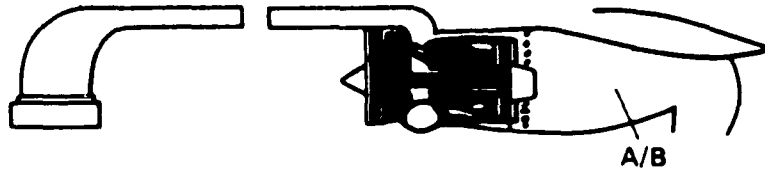


Figure 5. Remote Augmented Lift Propulsion Concept⁴

3.1.4 Ejector Augmentor Concept

In the ejector augmentor propulsion concept, vertical thrust is provided by two banks of ejectors and a ventral nozzle. The two banks of ejectors are supplied with fan air during vertical operations. The ventral nozzle is located on the cruise engine tailpipe and is supplied with turbine exhaust air. Turbine air is diverted from the main exhaust flow to the ventral nozzle by closing the throat area of the cruise nozzle. The cruise engine augmentor is not used during vertical operations. Figure 6 shows a schematic of the ejector augmentor propulsion concept.

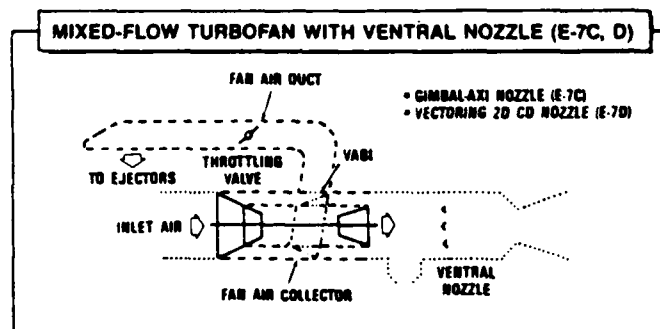


Figure 6. Ejector Augmentor Propulsion Concept¹⁷

3.1.5 HFVT Concept

In the HFVT propulsion concept, vertical thrust is developed by the two front fan nozzles and a vectoring cruise nozzle. The vectoring cruise nozzle is nonaugmented and directed down during vertical operations. The front nozzles are supplied with air from the front fan during vertical operations. Auxiliary inlets are used in the vertical flight mode to supply the gas generator fan with air. In the horizontal flight mode, the auxiliary inlets are closed and the front fan air is diverted from the front fan nozzles to the gas generator fan. Figure 7 shows the HFVT propulsion concept.

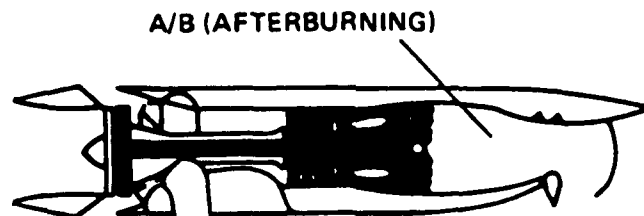


Figure 7. Hybrid Vectored Fan Thrust Propulsion Concept⁴

3.1.6 Lift Plus Lift/Cruise Concept

In the lift plus lift/cruise concept, vertical thrust is provided by one lift engine and a vectoring cruise nozzle. The cruise nozzle is vectored down during vertical operations. The lift/cruise engine exhaust is non-augmented during vertical flight but may be augmented in horizontal flight. Figure 8 shows the lift plus lift/cruise propulsion concept.

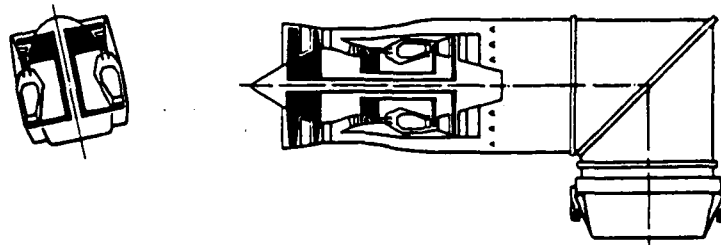


Figure 8. Lift Plus Lift/Cruise Propulsion Concept²²

3.2 Exhaust Characteristics of STOVL Propulsion Systems

The exhaust characteristics associated with the propulsion concepts discussed in section 3.1 are estimated in table 3. The table values represent exhaust conditions during vertical operations. Dry engine operation was estimated to produce exhaust conditions of $\text{NPR} = 4$ and $\text{EGT} = 1600^{\circ}\text{F}$. Augmented engine operation was assumed to produce exhaust conditions of $\text{NPR} = 4$ and $\text{EGT} = 3000^{\circ}\text{F}$. The ejector EGT was assumed to be 15°F higher than hot day ambient air.¹⁷ An isentropic relationship was used to calculate the HFVT EGT based on an inlet temperature of 103°F and a fan pressure ratio of four.

Table 3. STOVL Propulsion Exhaust Characteristics

Propulsion Concept	NPR	EGT (°F)	H/D at Touchdown
AV-8 ¹⁹			
Front Nozzles	2.0	260	4
Rear Nozzles	1.9	1350	2
Ejector Augmentor			
Ejectors	1.1	118	N/A
Ventral Nozzle	4	1600	3
Lift plus Lift/Cruise			
Lift Engine	4	1600	3
Vectored Cruise Nozzle	4	1600	3
RAL			
RAL Nozzles	4	3000	3
Vectored Cruise Nozzle	4	3000	3
REX			
REX Nozzles	4	1600	3
Ventral Nozzle	4	1600	3
HFVT			
Front Nozzles	4	375	3
Vectored Cruise Nozzle	4	1600	3

4.0 GROUND ENVIRONMENT ANALYSIS

STOVL propulsion systems create ground environments that may affect landing pads. Analysis methods, used to estimate ground environments and determine the effect they have on various landing pad materials, have been developed by NASA Ames, Naval Air Engineering Center, McDonnell Aircraft and British Aerospace. A detailed survey of these analyses was beyond the scope of this study, but a method was developed (see section 4.1) in this study to estimate the influence of propulsion system exhaust on landing pads. It was used to approximate the ground environments associated with the propulsion systems discussed in section 3.

These estimated ground environments and a preliminary assessment of the impacts they have on landing pad materials are discussed in section 4.2.

4.1 Ground Environment Analysis Methodology

Flow field characteristics, aerodynamic loads and thermal loads are the three main sections of the analysis. Flow field characteristics were studied to identify the parameters influencing the aerodynamic and thermal loads. STOVL propulsion flow field properties are discussed in section 4.1.1. The aerodynamic loads analyzed in this study are described in section 4.1.2. and the thermal loads are discussed in section 4.1.3. Assessments of the aerodynamic and thermal load analyses are provided in section 4.1.4.

4.1.1 Flow Field Characteristics

Parameters that influence flow fields include exhaust pressure, exhaust temperature, nozzle geometry, H/D ratio, aircraft sink rate, aircraft forward velocity and aircraft/engine configuration. A good understanding of the effects these parameters have on flow fields is essential to the development of an accurate ground environment analysis.

The exhaust jet that exists downstream of the nozzle and upstream of the ground interaction region may be viewed as a core surrounded by a mixing zone. The core total pressure is higher than ambient pressure and core total temperature is equivalent to the nozzle exit total temperature. Core length, influenced by nozzle pressure ratio and nozzle geometry, generally increases with nozzle pressure ratio. High mixing rate nozzles, such as

segmented types, tend to produce exhaust jets with shorter core lengths than axisymmetric nozzles. Large pressure variations may occur in the core zone due to the expansion that occurs in under-expanded exhaust jets. In the mixing zone, the ambient air interacts with the exhaust gases and diffuses the energy contained in the jet. The total pressure in the mixing zone approximates the ambient pressure and the mixing zone temperature is generally decreasing as the radial distance from the core zone increases. Mixing zone temperatures range from core zone to ambient levels. Figures 9 through 11 show axisymmetric nozzle free jet flow characteristics for various nozzle pressure ratios.

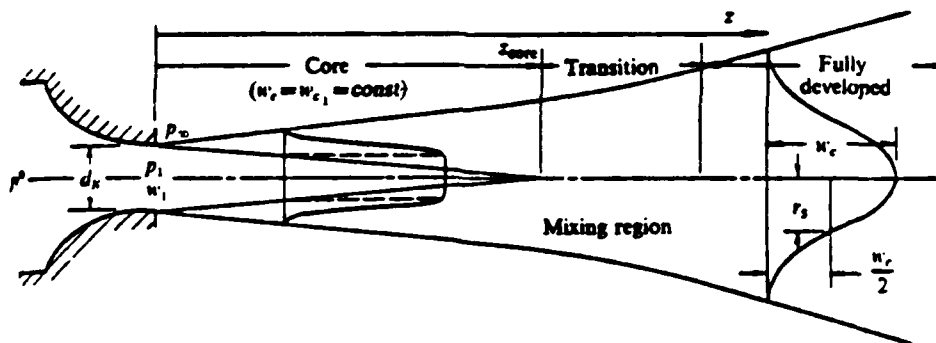


Figure 9. Jet Characteristics $\text{NPR} < 1.89$ -Subsonic Flow⁹

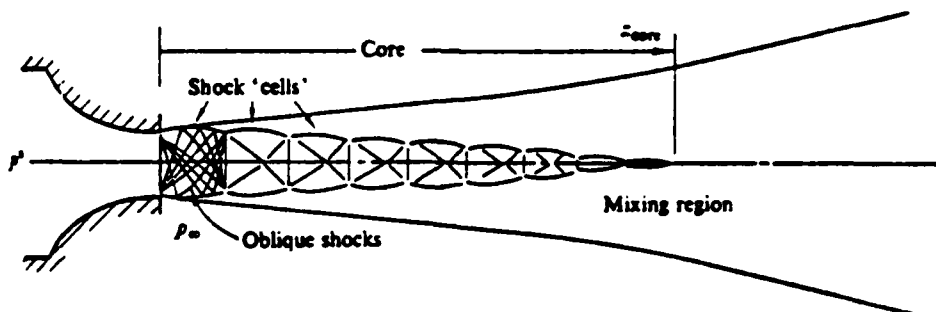


Figure 10. Jet Characteristics $2.1 < \text{NPR} < 3.85$ -Moderately Under-expanded Flow⁹

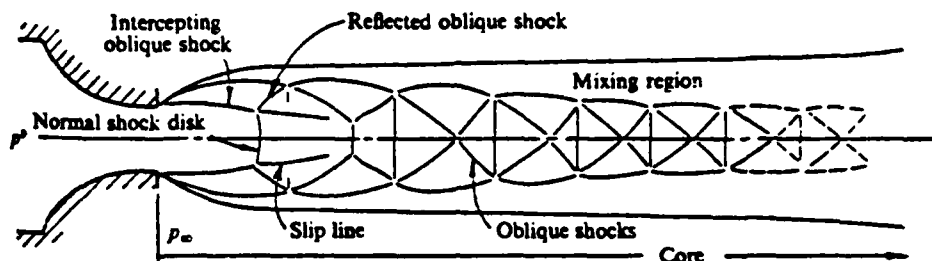


Figure 11. Jet Characteristics, $NPR > 3.85$ -Highly Under-expanded Flow⁹

When the free jet reaches the ground, an impingement region is formed, in which the direction of the jet exhaust is changed from vertical to horizontal. Exhaust gases expand radially outward from the center of the impingement zone. Shocks will be present in the impingement zone if the jet is underexpanded. The exhaust gases pass through the impingement zone and flow essentially parallel to the landing pad surface to form a wall jet. The thickness of the wall jet depends upon nozzle size, nozzle pressure ratio and radial distance from the impingement zone. Figure 12 shows two exhaust jets interacting with the ground. The structure of a supersonic jet impingement flow field is shown in figure 13.

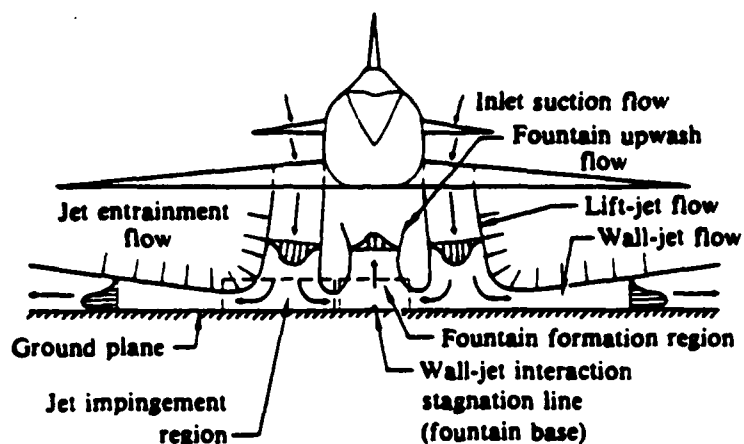


Figure 12. Exhaust Jet Impingement Flow Field³

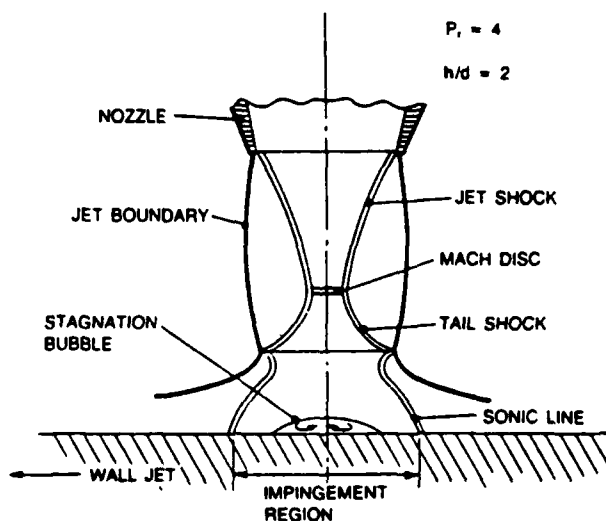


Figure 13. Supersonic Jet Impingement Flow Field¹⁹

Aircraft sink rate and forward velocity can effect jet impingement flow fields. An example of how aircraft forward velocity can affect jet flow fields is shown in figure 14.

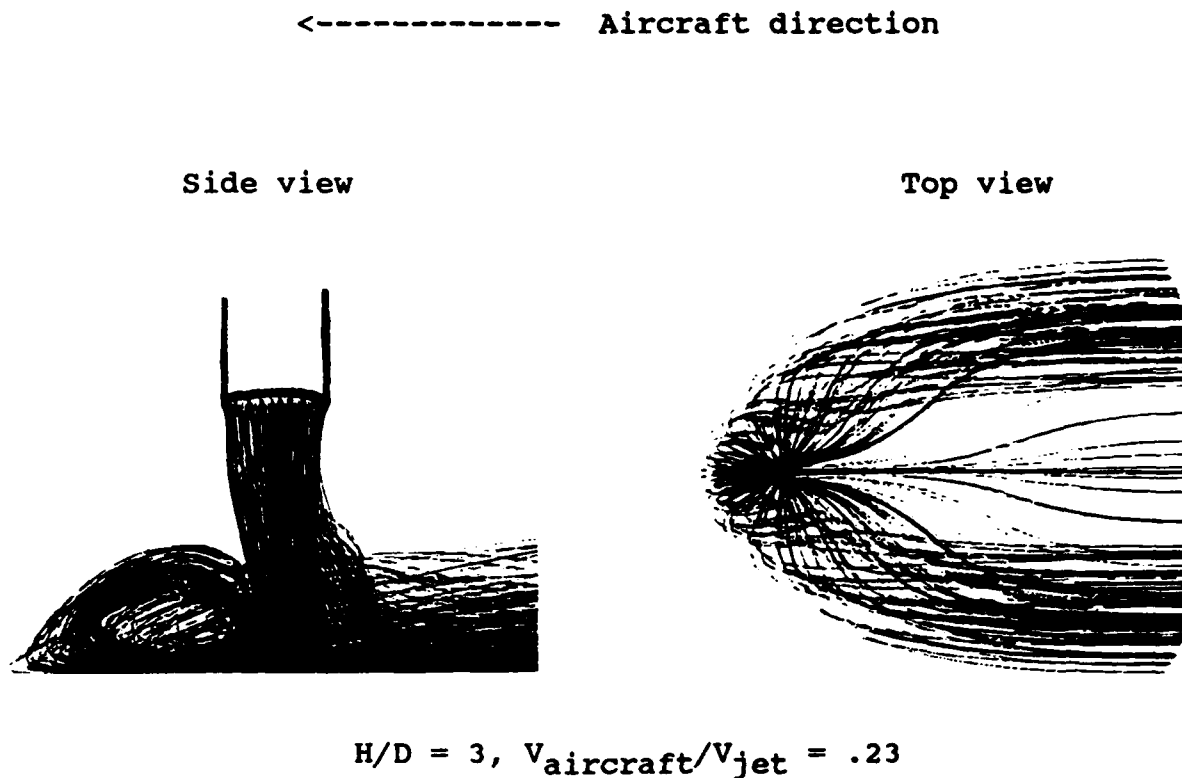


Figure 14. Jet Impingement Flow Field for Forward Moving Aircraft³⁵

4.1.2 Aerodynamic Loads

The aerodynamic loads exerted by jet exhaust on landing pads include pressure loads, shearing loads and jet-induced lifting loads. The aerodynamic loads investigated in this study include ground plane total pressure, ground plane dynamic pressure, ground plane shear stress and induced lifting forces. The ground plane total pressure is calculated first, followed by the ground plane dynamic pressure. Once the ground plane dynamic pressure is determined, the shear stresses and lifting forces can be calculated. Sections 4.1.2.1 through 4.1.2.4 discuss the procedures used to calculate the aerodynamic loads.

4.1.2.1 Ground Plane Total Pressure

Ground Plane total pressure is needed to estimate the compression load exerted by exhaust gases on a landing pad surface. Assuming the maximum normal pressure load exists at the center of the impingement zone, empirical data such as displayed in figure 15 may be used to estimate ground plane total pressure. Donaldson related impingement zone total pressure to nozzle exit conditions and ground proximity for axisymmetric nozzles (figure 15).⁹ If this information is used to estimate performance for non-circular exhaust systems, an "equivalent" nozzle diameter will be needed for an "equivalent" ground proximity. The maximum ground plane total pressure can be compared to the material normal pressure load limits in table 2 to determine if the landing pad will fail.

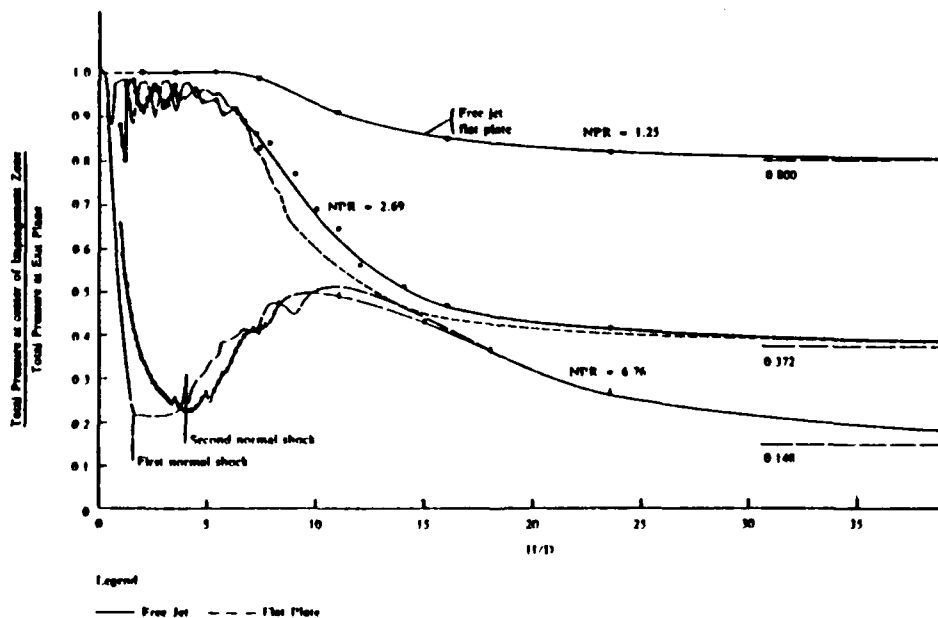


Figure 15. Axisymmetric Nozzle Ground Plane Total Pressure Curve

4.1.2.2 Ground Plane Dynamic Pressure

Ground plane dynamic pressure varies with H/D, nozzle geometry, nozzle pressure ratio and radial distance from the center of the impingement zone. The following equations were used to estimate the dynamic pressure:

$$Q = \frac{G}{2} \times P_s \times M^2 \qquad \frac{P_t}{P_s} = \left(1 + \frac{G-1}{2} \times M^2 \right)$$

Where:

Q = Dynamic pressure
G = Specific heat ratio = 1.4
M = Mach number
P_t = Total pressure
P_s = Static pressure

Combining the dynamic pressure expression with the isentropic pressure ratio/mach number equation and recognizing that Q/P_t is maximum at the square root of two, the relationship between total pressure and its associated dynamic pressure was determined. Using the ground plane total pressure, the related maximum dynamic pressure can be obtained from figure 16.

The calculated dynamic pressure can be compared to the material limits listed in table 2 to determine if the landing pad would be subject to erosion.

Lifting forces and shear stresses, the most likely causes of surface erosion, can be related to dynamic pressure. Expressions for these forces and stresses are developed in sections 4.1.2.3 and 4.1.2.4.

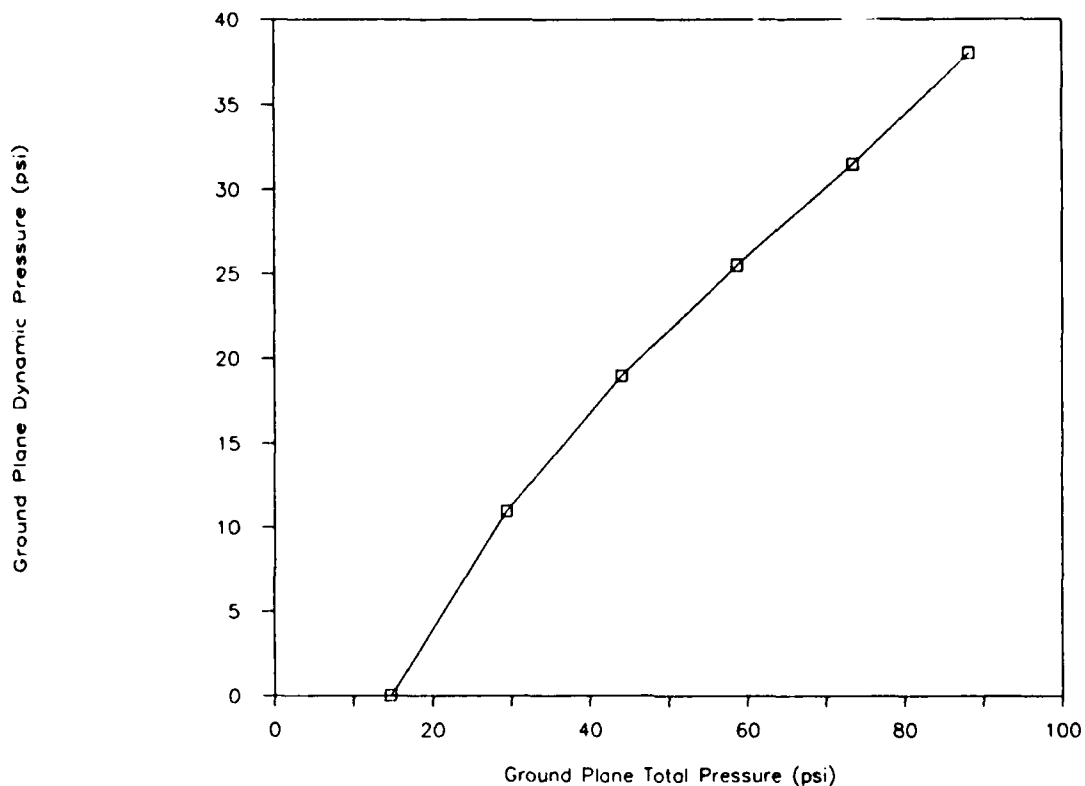


Figure 16. Ground Plane Dynamic Pressure

4.1.2.3 Ground Plane Shear Stress

Shear stress can be related to the dynamic pressure by the equation shown below:³²

$$S_h = C_f \times Q \quad C_f = \frac{.0262}{R_e^{.1428}}$$

Where:

- S_h = Shear stress
- C_f = Skin friction coefficient
- Q = Ground plane dynamic pressure
- R_e = Reynolds Number

The Reynolds number was set to 10,000,000 to approximate the turbulent flow conditions that exist at the maximum dynamic pressure condition. Ground plane dynamic pressure was varied to construct the curve shown in figure 17. This curve represents the maximum shear stress developed for a given dynamic pressure.

The ground plane dynamic pressure calculated in section 4.1.2.2 would be plotted on figure 17 to determine the shear stress level. The calculated shear stress can be compared to the material shear stress limits to determine if the landing pad will erode.

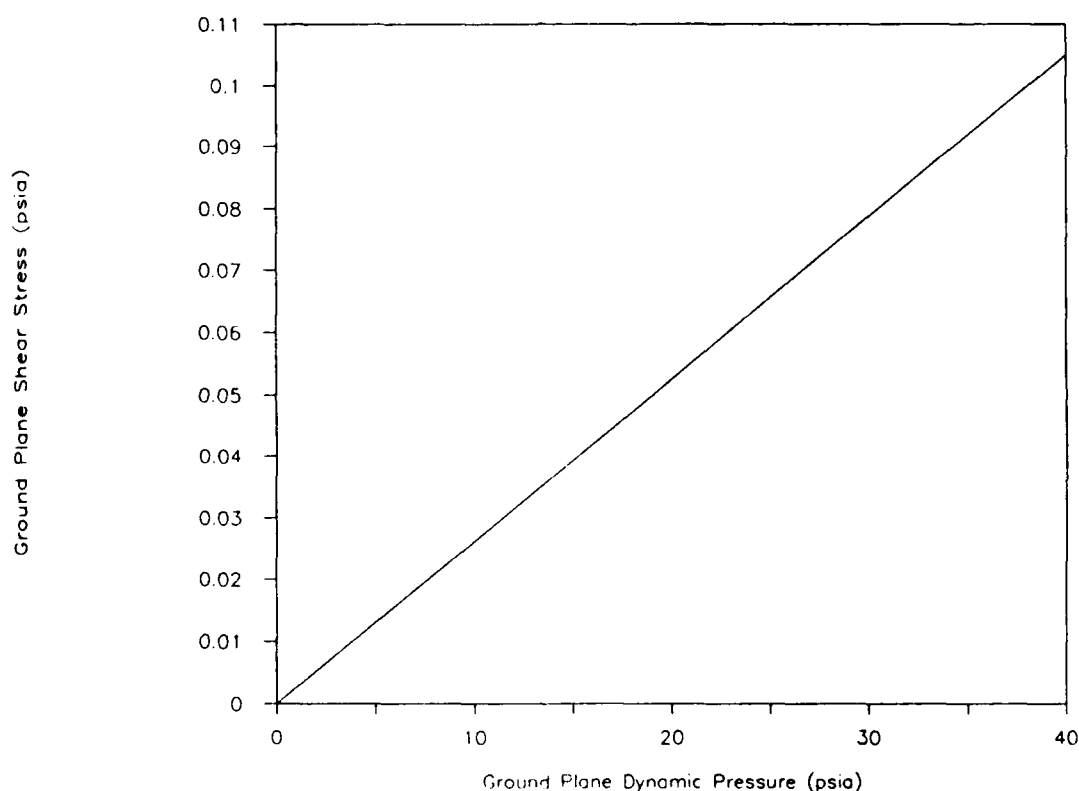


Figure 17. Ground Plane Shear Stress

4.1.2.4 Jet Induced Lift

Lifting forces can be generated by the exhaust jet as it flows over the landing pad. If a landing pad contains broken and loose pieces of pavement, the jet induced lifting forces may lift

those pieces. Lifting forces can be approximated with following equation:

$$L = \Delta C_p \times Q \times A_s$$

Where:

L = Lift
 ΔC_p = Change in the pressure coefficient over a surface
Q = Dynamic pressure
 A_s = Area of convex surface

A generic set of lifting forces curves was not developed in this study since insufficient information was available on the change in the pressure coefficient and the condition of the landing pad.

4.1.3. Thermal Loads

The procedures used to estimate thermal loads produced by jet exhaust address convection heat transfer, radiation heat transfer, conduction heat transfer, and thermal stress.

Convection and radiation heat transfer are calculated first. The total heat load applied to a landing pad is determined by summing the convection and radiation heat transfer rates. The total heat load is then input into the conduction analysis to determine the temperature profiles in the landing pad materials. The temperature gradients in the landing pad materials are used to estimate material thermal stresses and residence times.

4.1.3.1 Convection Heat Transfer

Convection heating is influenced by nozzle pressure ratio, exhaust gas temperature, nozzle geometry, aircraft sink rate, and aircraft velocity. The effects of nozzle pressure ratio and exhaust gas temperature were estimated in this analysis.

The exhaust nozzle was assumed to be at a H/D of six with no horizontal or vertical movement. At this height, the jet core would interact with the ground. The highest heat transfer rate occurs when the jet core impinges on the ground. The convection coefficient and convection heat transfer rate vary as the jet flows over the landing pad. The convection heat transfer rate can be estimated with the following equation:¹⁶

$$F_c = H \times (T_j - T_w)$$

Where:

F_c = Heat transfer rate
 H = Heat transfer coefficient
 T_j = Gas temperature at point of heat transfer estimate
 T_w = Landing pad surface temperature

The landing pad surface temperature was set to be a constant 100°F during the heating process. Even though the landing pad surface temperature increases under a heat load, the constant temperature simplification provides an initial estimate of the true heat transfer rate.

The heat transfer coefficient (H) was calculated with the following equation:¹⁶

$$H = S_t \times V_j \times D_n \times C_p$$

Where:

S_t = Stanton number
 V_j = Gas velocity at point of heat transfer estimate
 D_n = Gas density at point of heat transfer estimate
 C_p = Specific heat = .24 Btu/lb-°R

The Stanton number (S_t) was estimated with the Reynolds boundary layer analogy equation:¹⁶

$$S_t = \frac{C_f}{2}$$

Where:

C_f = Skin friction coefficient = $\frac{.0262}{R_e^{1/428}}$

This skin friction coefficient equation represents a turbulent boundary layer condition. The Reynolds number was assumed to be 10,000,000 for the analysis.

The gas velocity (V_j) was determined from the following equation:³⁴

$$V_j = M \times \sqrt{G \times C_a \times C_g \times T_t}$$

Where:

M = Mach number
 C_a = Gravitational constant = 32.17 lbm-ft/lbf-sec²
 C_g = Gas constant = 53.35 ft-lbf/^oR-lbm
 G = Specific heat ratio = 1.4
 T_t = Exhaust gas total temperature

The total temperature (T_t) was assumed to be equal to the total temperature of the exhaust gas at the nozzle exit. The mach number was calculated using the isentropic expression relating it to static and total pressures (see section 4.1.2.2.). The landing pad surface temperature (T_w) and the gas temperature at the point of the heat transfer estimate (T_j) were averaged to provide an average density for the heat transfer coefficient calculation. The gas density (D_n) can be calculated with the following equation:

$$D_n = P_j \times C_1 \times C_g \times \left(\frac{T_w + T_j}{2} \right)$$

Where:

P_j = Static pressure of exhaust at point of heat transfer estimate
 T_w = Landing pad surface temperature = 100^oF
 T_j = Gas temperature at point of heat transfer estimate
 C_g = Gas constant = 53.35 ft-lbf/^oR-lbm
 C_1 = Pressure unit conversion = 144 in²/ft²

The gas temperature (T_j) was determined with the following equation:³⁴

$$T_j = \frac{T_t}{\left(1 + \left(\frac{G-1}{2} \right) \times M^2 \right)}$$

Where:

T_t = Exhaust gas total temperature
 G = Specific heat ratio = 1.4
 M = Mach number

The total temperature (T_t) was assumed to be equal to the total temperature at the nozzle exit. The Mach number was set equal to that calculated in the gas velocity equation. Static pressure (P_j), ground plane total pressure (P_t) and ground plane total temperature were varied to construct convection heat transfer curves. The static pressure was varied to find the maximum heat transfer rate for each combination of ground plane total temperature and pressure. The convection curves are shown in figure 18. Ground plane total pressure determined in section 4.1.2.1 and the exhaust gas total temperature would be plotted on figure 18 to determine the convection heat transfer rate.

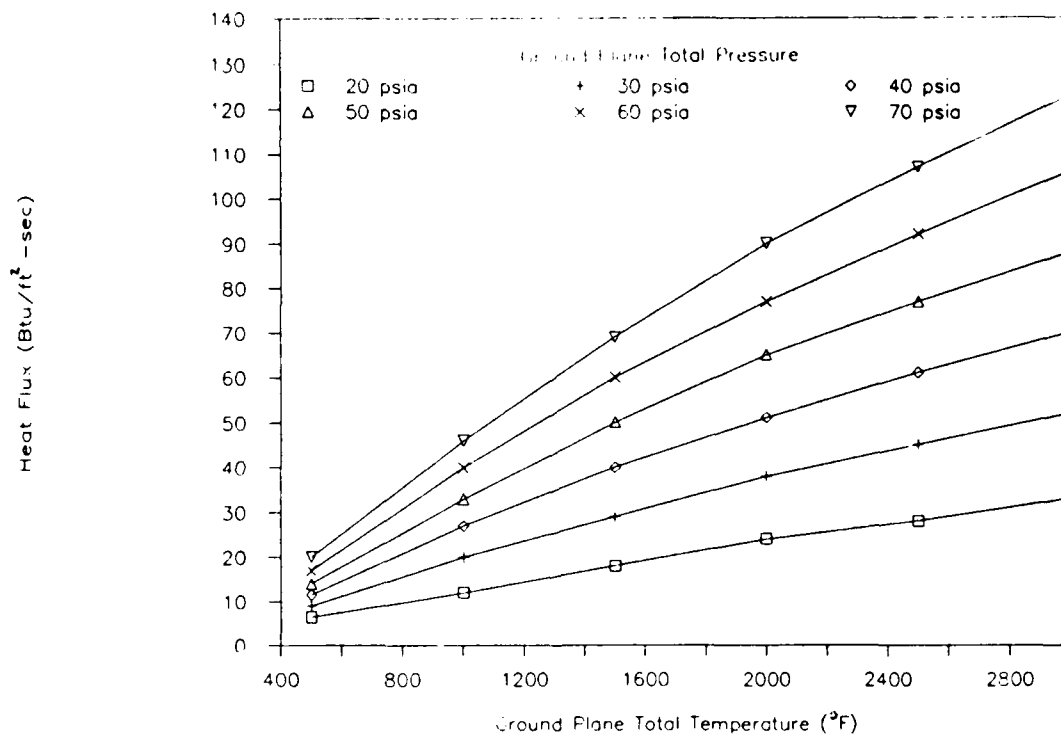


Figure 18. Convection Heat Transfer Rate

4.1.3.2 Radiation Heat Transfer

Radiation emitted from hot propulsion components and propulsion exhaust gases can affect landing pads. No information

was gathered on propulsion system component temperature levels or view factors, therefore, no heat transfer estimates were made for these components. Radiation heat transfer estimates are provided for the exhaust gases.

Radiation is emitted by carbon dioxide (CO_2) and water vapor (H_2O) molecules in exhaust gas. The concentration of CO_2 and H_2O must be known to determine the heat transfer rate.

Exhaust gas radiation is influenced by nozzle pressure ratio, exhaust gas temperature, combustion process, nozzle geometry, aircraft sink rate and aircraft forward velocity. The effects of nozzle pressure ratio and exhaust gas total temperature on the heat transfer rate were investigated in this study. The exhaust nozzle was assumed to be at a height corresponding to a H/D ratio of six. At this height, the jet core would be impinging on the ground. Radiation heat transfer can be calculated with the following equation:¹⁶

$$F_r = S_b \times (E_g \times T_g^4 - A_b \times T_w^4)$$

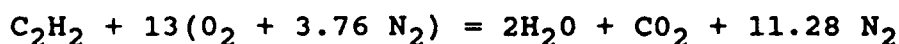
Where:

F_r = Radiation heat transfer
 S_b = Stefan Boltzman constant = 4.76×10^{-13} Btu/sec-ft²-°R
 E_g = Gas emissivity
 A_b = Gas absorptivity
 T_g = Gas temperature
 T_w = Landing pad surface temperature

The landing pad surface temperature was set to 100°F for this calculation. The surface temperature would increase with a heat load applied, but the constant temperature simplification provides an initial estimate of the radiation heat transfer rate. The gas temperature (T_g) was assumed to be equal to the exhaust gas total temperature at the nozzle exit. Kirchhoff's law was used to make gas absorptivity equivalent to gas emissivity.

Exhaust plume geometry must be estimated to determine the heat transfer rate. The plume was assumed to be cylindrical in shape with a height of 6 jet diameters and a base of 1 ft². Gas volume was calculated to be 6.77 ft³. The heat transfer rate was calculated for a 1 ft² section of the landing pad directly below the gas column. Total pressure, total temperature, beam lengths and partial pressures were used to determine the gas emissivity from figures 19 through 23. Partial pressures for CO₂ and H₂O were determined by analyzing the combustion process.

The stoichiometric combustion equation used in this analysis is shown below:³¹



H₂O and CO₂ partial pressures were calculated in the following manner:

$$\text{H}_2\text{O partial pressure: } P_w = \frac{2\text{H}_2\text{O}}{2\text{H}_2\text{O} + 2\text{CO}_2 + 11.28\text{N}_2} = \frac{2}{15.28} = .131$$

$$\text{CO}_2 \text{ partial pressure: } P_c = \frac{2\text{CO}_2}{2\text{H}_2\text{O} + 2\text{CO}_2 + 11.28\text{N}_2} = \frac{2}{15.28} = .131$$

The beam length associated with a gas column can be calculated with the equation shown below:¹⁶

$$\text{Beam Length (L)} = \frac{3.6 \times \text{Gas Volume}}{\text{Heated Ground Area}} = \frac{3.6 \times 6.77 \text{ ft}^3}{1 \text{ ft}^2} = 24.4 \text{ ft}$$

The partial pressures were multiplied by the beam length to determine the P_wL and P_cL graphing parameters.

The emissivity associated with the H₂O molecules was determined from figures 19 and 20. Figure 19 shows emissivity curves for H₂O at one atmosphere. P_wL and exhaust gas temperature T_g were plotted in figure 19 to find the emissivity. Since the water vapor in the jet core was at a pressure greater

than one atmosphere, a pressure correction factor was needed to adjust the water vapor emissivity.

The partial pressure of H_2O and the total exhaust pressure were averaged to determine the graphing parameter $(P_w + P)/2$. $P_w L$ and $(P_w + P)/2$ were plotted on figure 20 to find the pressure correction factor (C_w). The H_2O emissivity at one atmosphere was multiplied by C_w to determine the corrected emissivity, e_w .

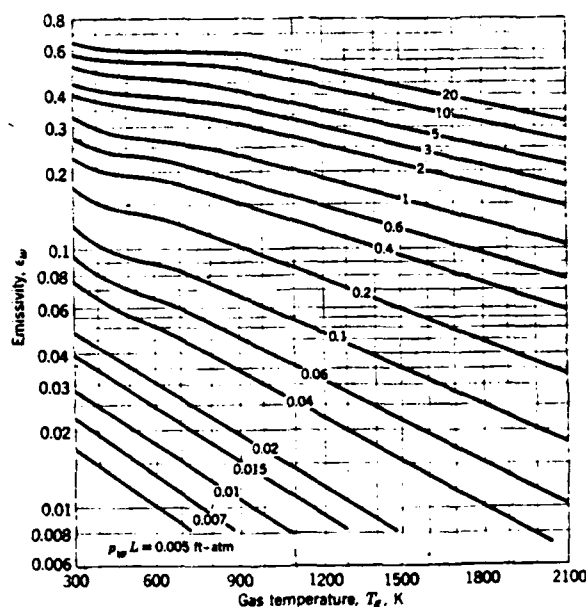


Figure 19. Water Vapor Emissivity at One Atmosphere¹⁶

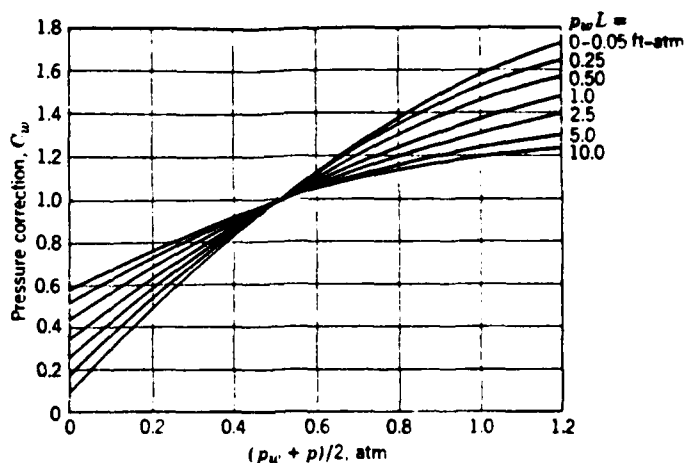


Figure 20. Water Vapor Pressure Correction Factor¹⁶

The emissivity associated with CO_2 molecules was determined from figures 21 and 22. Figure 21 shows the emissivity curves for CO_2 at one Atmosphere. $P_c L$ and exhaust gas temperature T_g were plotted on figure 21 to find the emissivity. Since the CO_2 in the jet core has a pressure higher than 1 atmosphere, a pressure correction factor was needed to adjust the CO_2 emissivity. $P_c L$ and the column exhaust gas total pressure (P_g) were plotted on figure 22 to find the pressure correction factor, C_c . The CO_2 emissivity at one atmosphere was multiplied by C_c to determine the corrected emissivity, e_c .

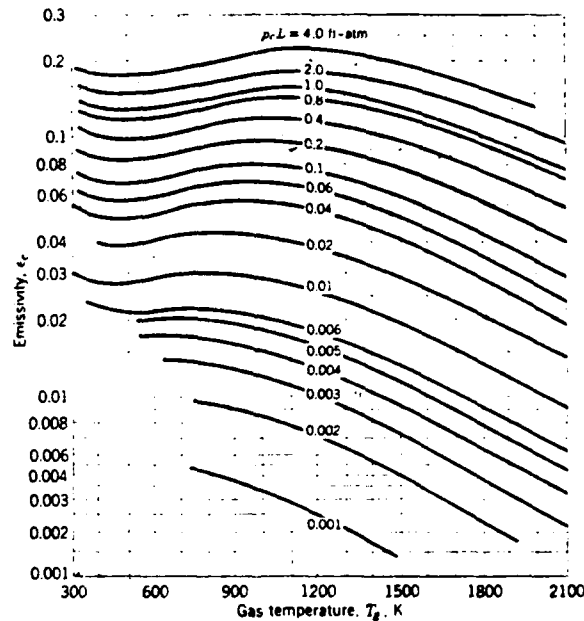


Figure 21. Carbon Dioxide Emissivity at One Atmosphere¹⁶

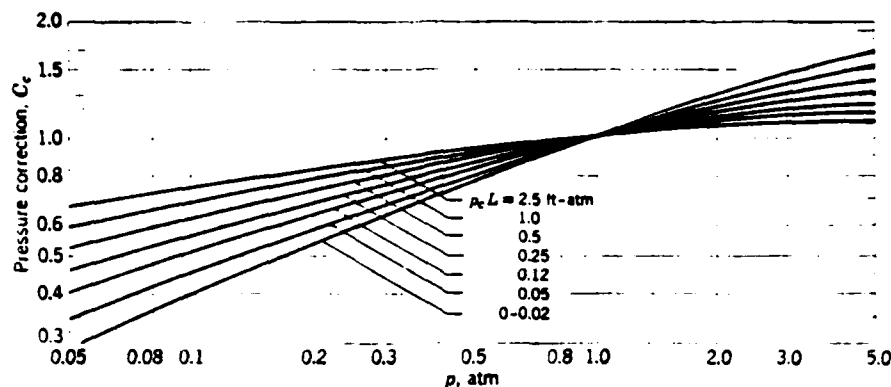


Figure 22. Carbon Dioxide Pressure Correction Factor¹⁶

The total emissivity for the gas column is calculated by adding the H₂O and CO₂ emissivities together. When the emissivities are added together, a mixture correction factor ($\Delta\epsilon$) must be applied. The beam length (L) is multiplied by the sum of the H₂O and CO₂ partial pressures to calculate the $L(P_W + P_C)$ parameter. The $P_W/(P_C + P_W)$ term is calculated by dividing the H₂O partial pressure by the sum of the H₂O and CO₂ partial pressures. Exhaust gas temperature (T_g), $P_W/(P_C + P_W)$ and $L(P_W + P_C)$ are plotted on figure 23 to find the mixture correction factor.

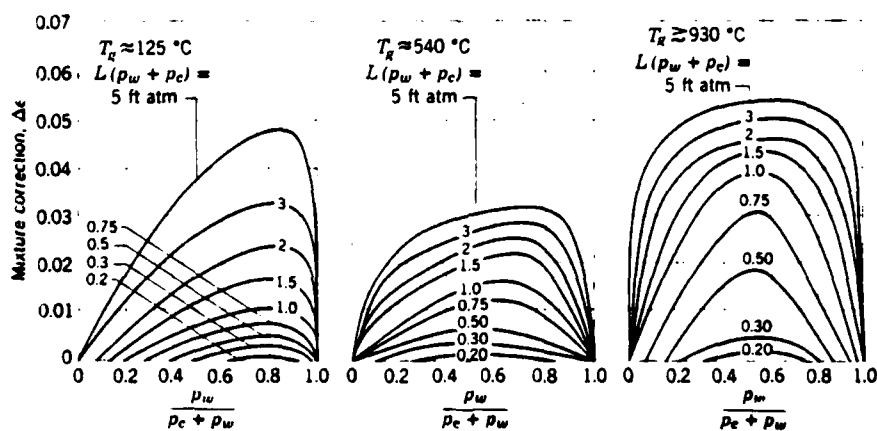


Figure 23. Mixture Correction Factor¹⁶

The equation used to determine the total emissivity of the exhaust as shown below:

$$E_g = e_w + e_c + \Delta e$$

Radiation heat transfer curves were constructed by varying the nozzle pressure ratio and the exhaust gas temperature. The radiation curves are shown in figure 24.

Propulsion system nozzle pressure ratio (NPR) and exhaust gas temperature can be plotted on figure 24 to determine the radiation heat transfer rate.

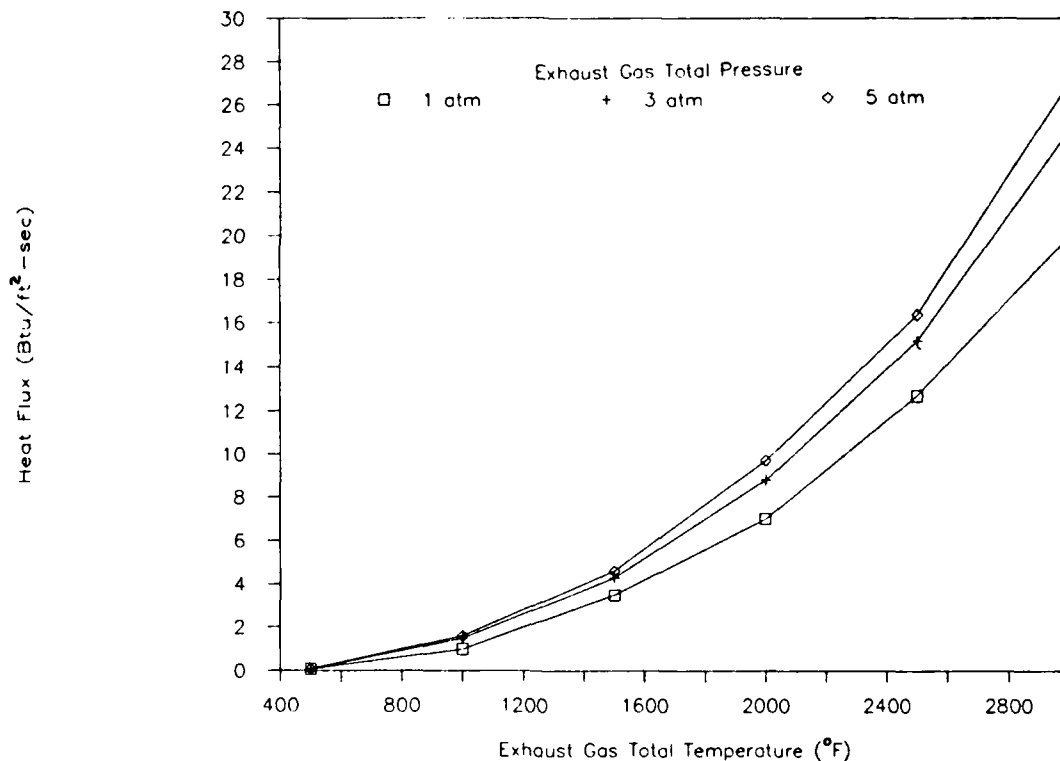


Figure 24. Radiation Heat Transfer (H/D=6)

4.1.3.3 Conduction Heat Transfer

A conduction analysis was done to determine the effect of convection and radiation heat loads on landing pad materials. In the analysis, the landing pad was assumed to be equivalent to a

semi-infinite solid exposed to a constant heat flux. Temperature profiles were developed for each landing pad material at various heat load conditions. The equation used to calculate the temperature profile is shown below:⁶

$$T_m = \frac{2 \times F_t}{K} \times \left(\frac{(D_i \times t)^5}{\pi} \times e^{-y^2/(4 \times D_i \times t)} - \frac{y}{2 \times \text{ERR}} \right) + T_o$$

Where:

T_m = Material temperature at depth y and time t
 F_t = Total heat flux (convection plus radiation)
 K = Thermal conductivity
 D_i = Thermal diffusivity
 t = Time
 y = Depth
 ERR = Conduction correction term
 T_o = Initial surface temperature

Thermal conductivities and thermal diffusivities for aluminum, asphalt concrete, PCC and steel were obtained from table 1. The conduction correction term (ERR) is influenced by material properties, depth into the material and time. ERFC was used to look up the ERR term listed in a table contained in "Conduction of Heat in Solids" by Carslew. The equation used to calculate ERFC is shown below:⁶

$$\text{ERFC} = \frac{y}{2 \times \sqrt{D_i \times t}}$$

Where:

y = Depth
 D_i = Thermal diffusivity
 t = Time

The initial surface temperature was set to 100°F to correspond the surface temperatures used in convection and radiation heat transfer calculations.

Total heat flux, time and depth were varied to determine the temperature profiles in the four landing pad materials under heat

loads of 10, 20, 30, 40, 50 and 60 Btu/ft²-sec. These temperature profiles are located in appendix A. An example temperature profile is shown in figure 25.

The temperature profiles can be used to estimate surface temperature, temperature gradients and residence time limits. The calculated surface material temperatures can be compared to the temperature limits shown in table 2 to determine if the landing pads will fail under the applied heat load. Residence time limits can be found by calculating the time required to heat up the landing pad to the failure point.

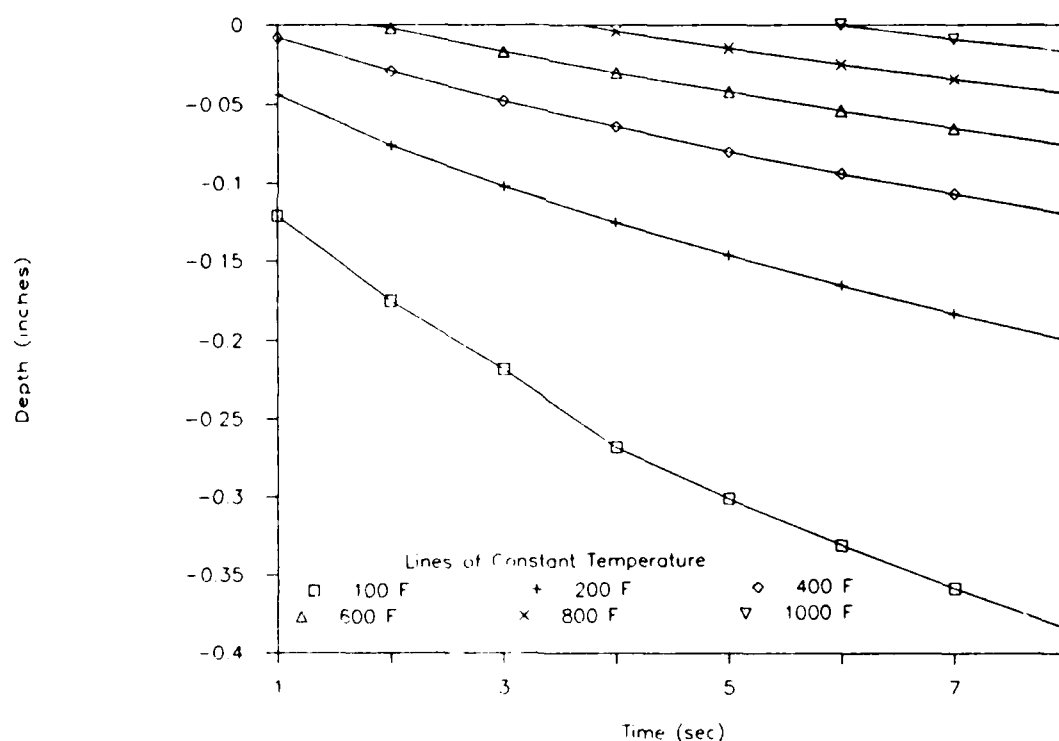


Figure 25. Temperature Profiles in PCC -30 Btu/ft²-sec

4.1.3.4 Thermal Stress

Thermal stress calculations can be performed to understand material failure mechanisms. A preliminary stress analysis was conducted in this study. The analysis assumed that the landing

pad was fully constrained (no expansion allowed). Thermal stress may be calculated with the following equations:

$$S_{th} = \frac{\Delta L}{L} \times E$$

$$\frac{\Delta L}{L} = E_x \times (T_m - T_o)$$

Where:

S_{th} = Thermal stress

E = Modulus of elasticity

E_x = Thermal expansion coefficient

T_t = Final material temperature

T_o = Initial material temperature

The moduli of elasticity and thermal expansion coefficients for each material were obtained from table 1. The final material temperature was varied to construct thermal stress curves for aluminum, asphalt concrete, PCC and steel. Figures 26 through 29 show the thermal stress curves calculated for the landing pad materials. The difference between the initial material temperature and the final material temperature would be plotted on the stress curves to find the stress level in the material. The stress level can be compared to the material compression load limits shown in table 1 to determine if the material will fail. The thermal stress analysis did not correlate well with the failures experienced on landing pads and will need to be restudied.

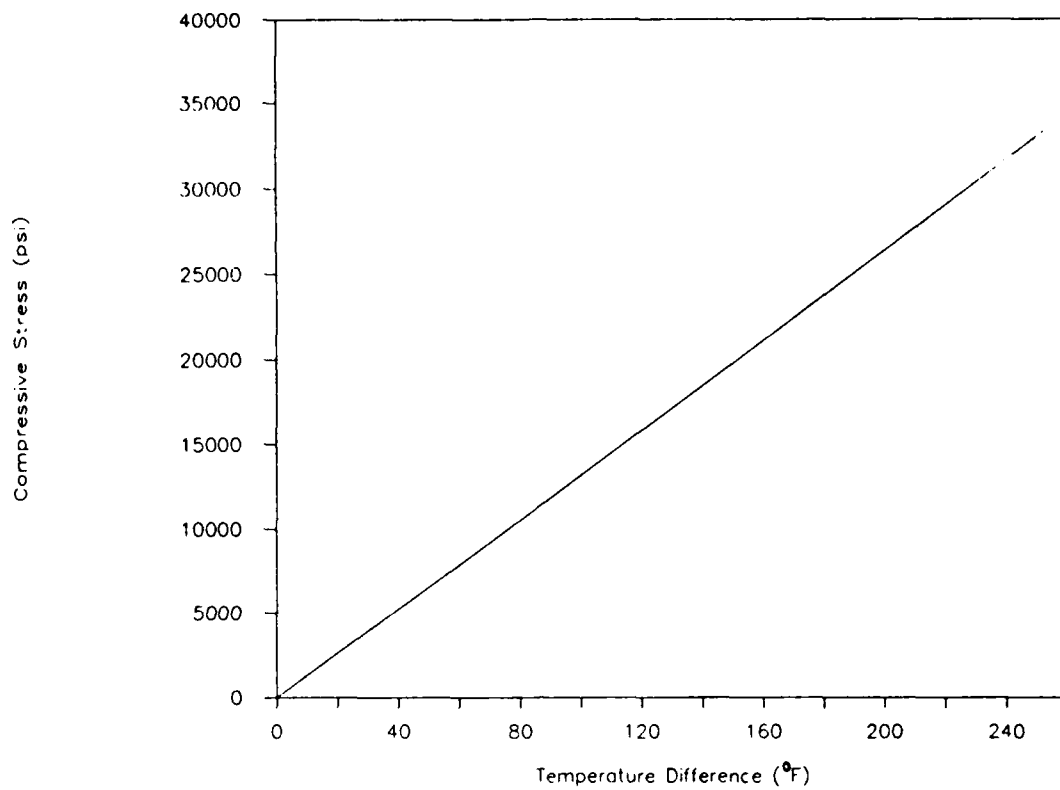


Figure 26. Thermal Stress in Aluminum

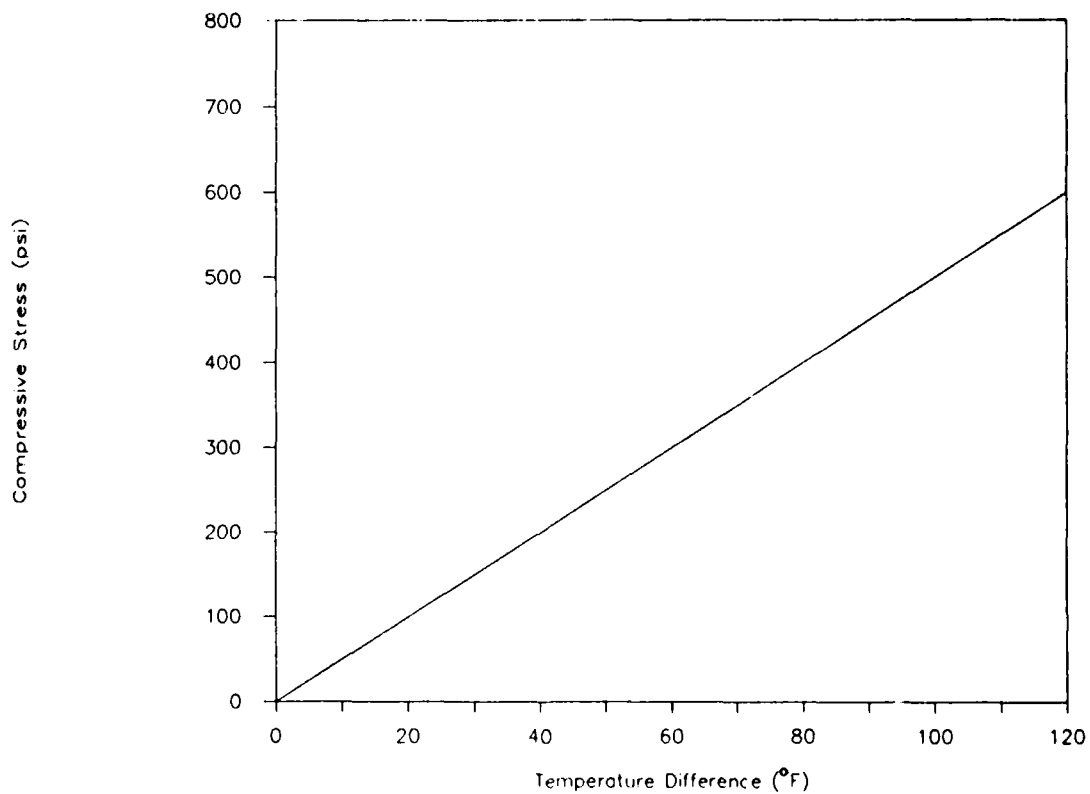


Figure 27. Thermal Stress in Asphalt Concrete

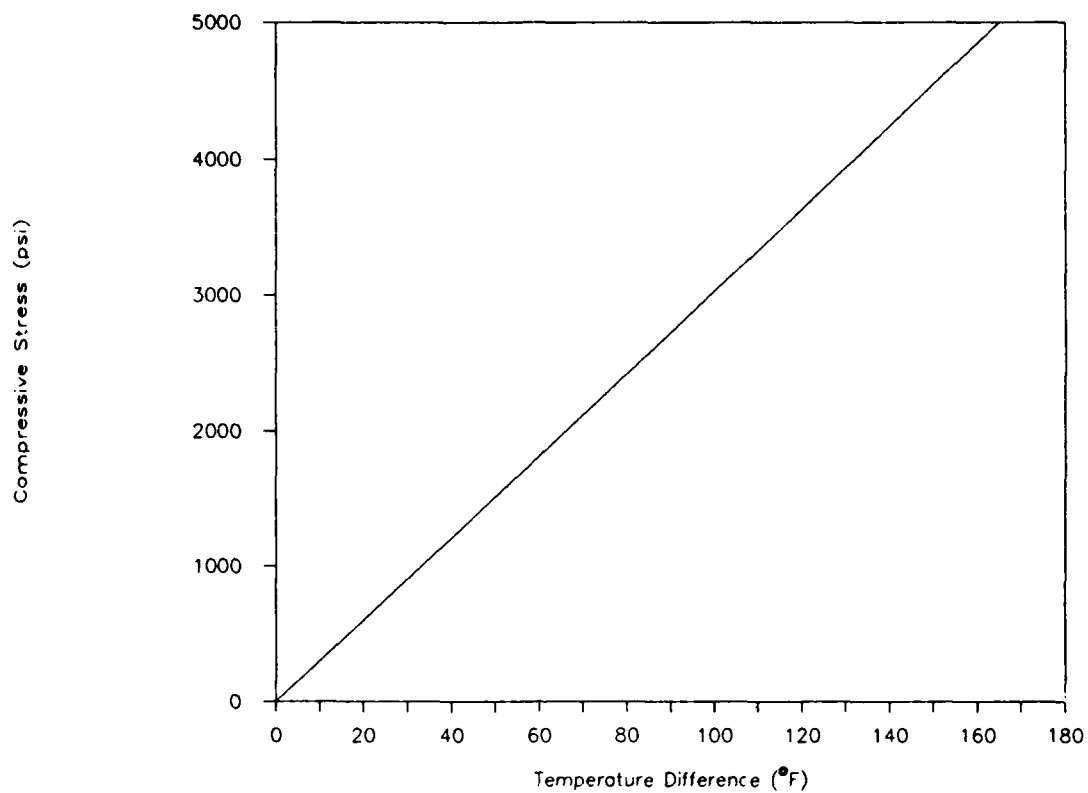


Figure 28. Thermal Stress in PCC

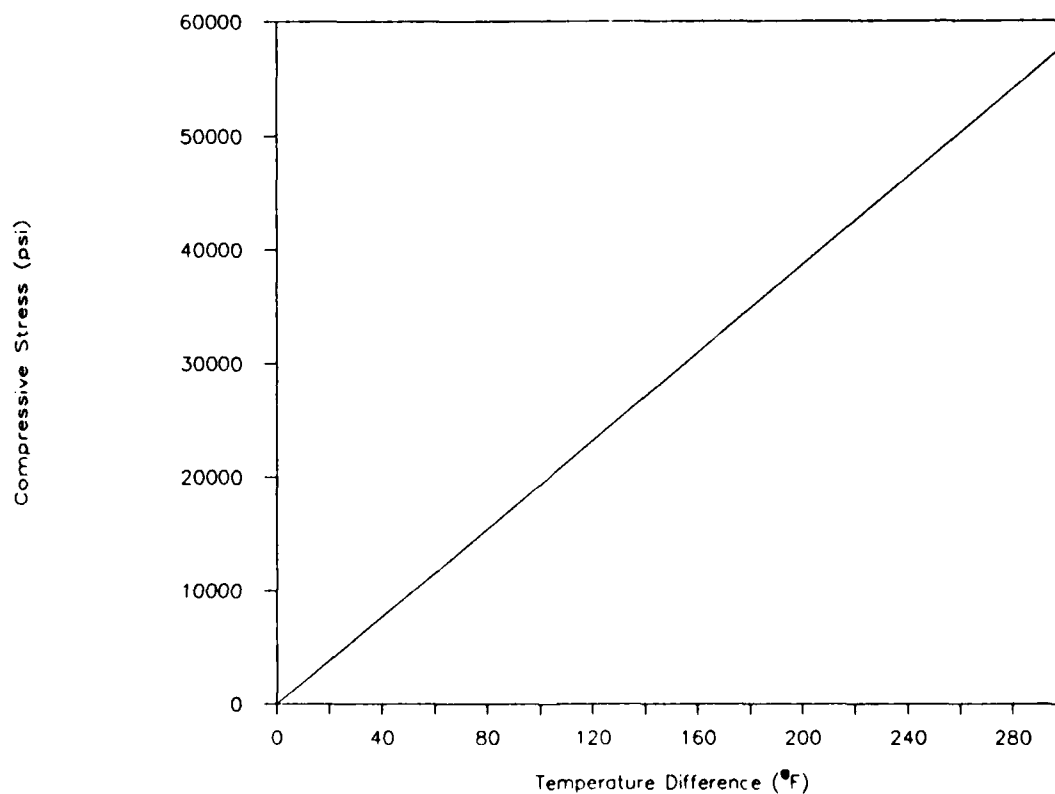


Figure 29. Thermal Stress in Steel

4.1.4 Load Assessment

An initial assessment of the aerodynamic and thermal loads discussed in this study is given in sections 4.1.4.1 and 4.1.4.2.

4.1.4.1 Aerodynamic Loads

The aerodynamic pressure loads produced by jet exhaust may damage landing pad materials. Normal pressure loads were low compared to the material compressive strengths and should not damage the landing pads. The shear stresses produced by jet flow are too low to cause erosion. Lifting forces may be of sufficient strength to move loose pieces of pavement or dislodge PCC joint filler. The capability to predict the effect of lifting loads on landing pads is important and should be further studied.

4.1.4.2 Thermal Loads

The thermal loads produced by jet exhaust may damage landing pad materials. Convection heating provides the greatest source of heat but radiation can also have an important impact on the heating rate. Asphalt concretes and PCC joint fillers are easily affected by high temperatures. PCC has a higher tolerance for heating than asphalt concrete but is not as resistant as thick steel or thick aluminum. The heating loads applied to a landing pad may be lowered by landing the aircraft with a forward velocity and a high sink rate. The effect heating loads have on landing pads is important and should be studied in greater detail.

4.2 Propulsion Concept Ground Environment Ratings

Preliminary estimates of the ground environments produced by the six propulsion concepts described in section 3 were made in this study. The propulsion exhaust characteristics shown in table 3 were input into the analysis method described in section 4.1. Aerodynamic and thermal loads were calculated for the propulsion concepts. Section 4.2.1 discusses the aerodynamic loads and section 4.2.2 discusses the thermal loads. An initial ranking of the propulsion concept ground environments is given in section 4.2.3.

4.2.1 Propulsion Concept Aerodynamic Loads

Ground plane total and dynamic pressures were estimated for the propulsion concepts. The procedures described in section 4.1.2.1 were used to determine the ground plane total pressure. Ground plane dynamic pressure was calculated with the procedures described in section 4.1.2.2. The estimated ground plane total pressure and dynamic pressure are shown in table 4.

Table 4. Propulsion System Pressure Estimates

Concept	Ground Plane Total Pressure (psi)	Ground Plane Dynamic Pressure (psi)
AV-8	28	10.5
Ejector	36	14
HFVT		
REX		
Lift Plus lift/cruise		
RAL		

Shear stress estimates were not made for the propulsion concepts since the analysis in section 4.1.2.3 showed that stresses would be small. Lifting loads were not estimated for the propulsion concepts due to the problems discussed in section 4.1.2.4.

4.2.2 Propulsion Concept Thermal Loads

Convection heating estimates were determined using the procedures listed in section 4.1.3.1. The heat produced by radiation was calculated with the procedures listed in section 4.1.3.2. Table 5 shows the convection, radiation and total heat load produced by each propulsion system.

Table 5. Propulsion System Heat Transfer Estimates

Propulsion Concept	Convection Heating Estimates (Btu/ft ² -sec)	Radiation Heating Estimates (Btu/ft ² -sec)	Total Heating Estimates (Btu/ft ² -sec)
AV-8	22	3	25
Ejector Augmentor	} 63	} 5	} 68
HFVT			
REX			
Lift plus lift/cruise			
RAL	105	26	131

Thermal stresses were not estimated for the propulsion systems due to the reasons discussed in section 4.1.4.2. Estimated residence time limits were determined using the procedures described in section 4.1.3.3. The aircraft was assumed to be stationary over the landing pad for the residence time estimates shown in table 6.

Table 6. Residence Time Limits

Propulsion Concept	Residence Time Limit (seconds)			
	Aluminum	Asphalt Concrete	PCC	Steel
AV-8	65	1	3	45
Ejector Augmentor	} 27	} <1	} <1	} 22
HFVT				
REX				
Lift plus lift/cruise				
RAL	<1	<1	<1	<1

4.2.3 Propulsion Concept Ranking

The residence times indicated that the heat flux generated by a propulsion system was the limiting factor. Aerodynamic forces such as normal pressure loads and shear stresses were not large enough to be considered a major factor. Lifting forces were ignored since insufficient information was obtained on these forces.

Propulsion systems were ranked from the most severe to the least severe ground environment in table 7. The ranking was based on the total heat flux values shown in table 5. The ranking will require revision as the propulsion systems are developed and the analysis methods are improved.

Table 7. Propulsion Concept Ranking

Propulsion Concept	Index	Rank
RAL	1	1
Lift plus lift/cruise	} 6	} 2
Ejector Augmentor		
REX		
HFVT		
AV-8	10	3

5.0 GROUND ENVIRONMENT TEST FACILITIES

Sub and full-scale ground environment testing will be necessary on future STOVL aircraft development programs. Test facility requirements are needed to identify the facilities capable of conducting ground environment testing. Preliminary requirements for test facilities are discussed in section 5.1 and section 5.2 identifies test facilities that may suffice for future STOVL aircraft research programs. The facilities possessing the capabilities that best matched the preliminary requirements are discussed in section 5.3.

5.1 Preliminary Test Facility Capability Requirements

Preliminary capability requirements were identified from information gathered on propulsion system exhaust parameters and aircraft landing operations. The requirements will need updating as research proceeds on STOVL aircraft. The preliminary test facility requirements are shown in table 8.

Table 8. Preliminary Test Facility Requirements

Parameter	Range
Exhaust pressure ratio	1 to 6
Exhaust temperature	0°F to 3000°F
H/D	1 to 10
Sink rate	0 ft/sec to 10 ft/sec
Forward velocity	0 ft/sec to 30 ft/sec
Ground material	Asphalt, Steel, Aluminum, PCC
Ground material surface temperature	0°F to 1500°F
Ground plane pressure sensors	14 psia to 100 psia
Ground plane temperature sensors	0°F to 3000°F
Ground plane velocity sensors	0 ft/sec to 2000 ft/sec

All these capabilities may not be available at one facility, therefore, testing could be split up among various facilities to obtain the needed data. Scaling relations will need to be developed for model testing. The relationships between nozzle exhaust conditions, nozzle size and the size of the landing pad test sample will need to be investigated. Once the applicability of the scaling factors has been determined, the split between full-scale and sub-scale testing can be made.

5.2 Identified Test Facilities

Facilities that could conceivably be used for STOVL ground environment studies are identified in this section. Full-scale facilities are listed in table 9. Table 10 lists the sub-scale test facilities. Test capabilities and potential uses for each facility are included in the tables.

Test cell modifications may be required to effectively use the identified facilities. Some figures of the identified test facilities are included in appendix B.

Table 9. Full-Scale Test Facilities

Facility	Capabilities	Possible Uses
J-85 Movable Engine Test Rig ²⁵	Full-size engine Variable engine attitude Variable engine height Engine can be moved over selected landing pad materials	Flow field tests Heat transfer tests Ground erosion tests
NASA Ames 80 X 120 Wind Tunnel ²⁷	Full-size aircraft Adjustable height Engines can be run	Flow field tests Heat transfer tests

Table 9. Full-Scale Test Facilities - Continued

Facility	Capabilities	Possible Uses
NASA Ames Outdoor Aerodynamic Research Facility ²⁷	Full-size aircraft Adjustable height by crane	Flow field tests Heat transfer tests Ground erosion tests
NASA Lewis Powered Lift Facility	Full-size engine Adjustable engine height Needs design for vertical engine mount	Flow field tests Heat transfer tests Ground erosion tests
Naval Aero Propulsion Center Gyro-rig ¹²	Full-size engine Engine can be rotated past sample test panels to simulate aircraft forward velocity Test panel mounting system needed	Flow field tests Heat transfer tests Ground erosion tests
Naval Aero Propulsion Center Variable Attitude Rig ¹²	Full-size engine Adjustable engine height Test panel mounting system needed for height adjustment	Flow field tests Heat transfer tests Ground erosion tests
Naval Air Engineering Center J-79 Erosion Rig ¹⁰	Full-size engine mounted horizontally Test panels mounted behind the engine	Flow field tests Heat transfer tests Ground erosion tests
Rolls-Royce Shoeburyness Facility ¹¹	Full-size aircraft Ground plane instrumentation Dynamic landing simulation	Flow field tests Heat transfer tests Ground erosion tests
Rolls-Royce RB108 Ground Erosion Rig ¹³	Full-size engine Movable gantry Adjustable engine height and attitude	Flow field tests Heat transfer tests Ground erosion tests

Table 10. Sub-Scale Model Test Facilities

Facility	Capabilities	Possible Uses
NASA Ames 40 X 80 Wind Tunnel ²⁷	Large model aircraft Model height adjustable Engines can be run	Flow field tests Heat transfer tests
NASA Langley 30 X 60 Wind Tunnel ²⁰	Large model aircraft Model height adjustable	Flow field tests Heat transfer tests
NASA Langley 4 X 7 Wind Tunnel ²⁰	Large model aircraft Model height adjustable Moving belt ground plane Nozzle pressure ratio = 4 cold flow	Flow field tests
NASA Lewis 9 X 15 Wind Tunnel ¹⁸	Small model aircraft Ground plane height adjustable Ground plane instrumentation Maximum EGT = 1000°F	Flow field tests Heat transfer tests
Boeing V/STOVL Wind Tunnel ²⁰	Small model aircraft Model height adjustable Moving belt ground plane	Flow field tests Heat transfer tests
Boeing Cold Air Rig ¹⁵	Large model nozzles Ground plane height adjustable Ground plane instrumentation Nozzle pressure ratio= 2.5 cold flow	Flow field tests
British Aerospace Low Speed Wind Tunnel ³⁰	Large model aircraft Model height adjustable	Flow field tests
British Aerospace Hot Gas Ingestion Facility ⁵	Small model aircraft Model height adjustable Ground plane instrumentation	Flow field tests Heat transfer tests

Table 10. Sub-Scale Model Test Facilities - Continued

Facilities	Capabilities	Possible Uses
British Aerospace Warton Hot Gas Lab Ground Erosion Rig ¹⁹	Large model burner and nozzle Nozzle Pressure ratio = 4 Maximum EGT = 2200°F Ground plane instrumentation	Flow field tests Heat transfer tests Ground erosion tests
German-Dutch DWN Low Speed Wind Tunnel ²⁰	Large model aircraft Model height adjustable	Flow field tests
McDonnell Aircraft Jet Interaction Apparatus ²¹	Small model aircraft and nozzles Ground plane height adjustable Ground plane instrumentation Nozzle pressure ratio = 3 cold flow	Flow field tests Heat transfer tests
Pennsylvania State University Applied Research Lab ⁷	Small model nozzle Ground plane height adjustable Ground plane instrumentation Nozzle pressure ratio = 2 cold flow	Flow field tests Heat transfer tests
Portland Cement Association CTL Fire Test Cells ⁸	High temperature testing of concrete	Ground erosion tests
Sandia Laboratory ²⁶	High temperature testing of concrete Test panel instrumentation Nozzle pressure ratio = 4 Maximum EGT = 3000°F	Ground erosion tests

5.3 Test Facilities Suggested for Future Research

A review of the facilities discussed in section 5.2 revealed two sub-scale facilities and two full-scale facilities that best

matched the test facility requirements discussed in Section 5.1. The Warton Hot Gas Facility and the NASA Lewis 9 X 15 wind tunnel are suggested for sub-scale model testing. The Warton facility has an erosion rig which can simulate exhaust pressure and temperature, H/D ratios and residence times. Test samples can be changed to evaluate different landing pad materials. The Warton facility is located in the United Kingdom and the United States may not have access to this facility but a similar facility could be set up in the United States. The NASA Lewis facility has the capability to simulate exhaust pressure and temperature, H/D ratios, and forward aircraft movement. The Lewis facility has been used to study hot gas ingestion on STOVL aircraft models.

The two full-scale facilities suggested for future test programs were the Rolls-Royce RB108 rig and the NASA Ames 80 X 120 wind tunnel. The Rolls-Royce rig is a movable gantry that can hold a full-scale engine. Engine height and attitude can be adjusted in the gantry. This rig can be positioned over various landing pad types to determine a materials response to jet blast. The United States may not have access to this rig since it is located in United Kingdom but a similar rig could be set up in the United States. The NASA Ames 80 X 120 wind tunnel has the capability to test full-scale aircraft. Full sized engines could possibly be run in the test aircraft. Forward aircraft movement and H/D ratios can be simulated in the Ames facility.

These suggestions need updating as further information is gathered on ground environment test requirements and test facility capabilities.

6.0 CONCLUSIONS

The analyses conducted in this study indicate that STOVL aircraft ground environments can damage landing pads if aircraft landing procedures are not correctly defined or followed. Each aircraft/propulsion concept produces a ground environment which affects the landing pad according to the severity of the exhaust gas flow field. Ground environments are therefore an important design parameter for aircraft and propulsion systems developer.

Preliminary landing pad environmental limits were compared to the aerodynamic and heat loads estimated for the various STOVL aircraft/propulsion concepts. Pressure loads were determined to be insufficient to damage the baseline landing pads, but under the right conditions, broken pavement and loose joint filler can be lifted by high velocity exhaust gases. Propulsion system exhaust gases are capable of producing thermal stresses and temperatures in landing pads that surpass the material failure limits. Jet residence time limits are necessary to prevent thermal damage to landing pads. The preliminary residence time limits calculated in this study show that rolling landings are needed on asphalt concrete and PCC. Rolling landings may also be required on steel and aluminum pads if a RAL system is selected or if repetitive vertical operations are conducted with the other propulsion concepts.

Data that accurately defines landing pad environmental limits and analyses that predict STOVL aircraft ground environment severity are needed. Testing and analysis can be

conducted to determine landing pad failure limits and improve ground environment load estimates. Variables that should be evaluated in a test and analysis research program are shown in table 11. Test facilities best suited for future research programs, as determined in this study, include the Warton Hot Gas Laboratory Ground Erosion Rig, NASA Lewis 9 X 15 low speed wind tunnel, Rolls-Royce RB108 engine gantry and NASA Ames 80 X 120 low speed wind tunnel.

Table 11. Test Parameters

Test Parameter	Test Range
Nozzle pressure ratio	1 to 6
Exhaust gas temperature	100°F to 3000°F
H/D ratio	1 to 10
Aircraft sink rate	0 to 10 ft/sec
Aircraft forward velocity	0 to 30 ft/sec
Nozzle geometry	Round, Rectangular, Segmented
Landing Pad Material	Aluminum, Asphalt, PCC, Steel
Nozzle Area	1 ft ² to 3 ft ²

7.0 RECOMMENDATIONS

Based on the analyses and assessments conducted in this study the following recommendations have been made for future research efforts.

- o Conduct tests to investigate the heat and aerodynamic loads associated with future STOVL propulsion systems and determine the effect these loads have on typical landing pad materials. The parameters that should be investigated in a STOVL ground environment test program are shown in table 11. Some full-scale testing should be done up front to ensure scaling factors are properly set for sub-scale model tests. The Warton Hot Gas Laboratory Ground Erosion Rig and the NASA Lewis 9 X 15 wind tunnel are suggested for sub-scale test programs while the Rolls-Royce RB108 engine gantry rig and the NASA Ames 80 X 120 wind tunnel are recommended for full-scale test programs.
- o Develop an analysis method that can accurately predict STOVL propulsion ground environments and the effect they have on landing pad materials. The analysis will need to be able to evaluate various propulsion concepts. Variables such as nozzle exhaust pressure, exhaust gas temperature, nozzle diameter, H/D, nozzle geometry, aircraft sink rate, aircraft forward velocity and landing material type should be modeled in the analysis method.

REFERENCES

1. Abraham, Herbert. "Bituminous Paving Materials." Asphalts and Allied Substances, Vol. 3. Princeton, NJ: D. Van Nostrand Company, Inc., 1962.
2. Abrams, M. S. Compressive Strength of Concrete at Temperatures to 1,600F. (RD016.01T) Portland Cement Association, 1973.
3. Agarwal, Ramesh K. "Recent Advances in Prediction Methods for Jet-Induced Effects of V/STOL Aircraft." Recent Advances in Aerodynamics. Anjaneyulu Krothpalli and Charles A. Smith, Eds. New York: Springer-Verlag, 1986. 471-521.
4. Armstrong, Frank W. and Jack Lewis. "Overview of the US/UK ASTOVL Program." Proceedings of the International Powered Lift Conference. Warrendale, PA: Society of Automotive Engineers, Feb. 1988.
5. Bore, C. L. "Ground Based Testing Without Wind Tunnels." AGARD-R-710 Special Course on V/STOL Aerodynamics. Apr. 1984.
6. Carslew, H. S. and J. C. Jaeger. Conduction of Heat in Solids. Oxford, 1960.
7. Cimbala, J. M., et al. "Experimental Investigation of a Jet Impinging on a on a Ground Plane in the Presence of a Cross Flow." Proceedings of the International Powered Lift Conference. Warrendale, PA: Society of Automotive Engineering, Feb. 1988.
8. Construction Technology Laboratories, Inc. Catalog of Professional Services. Skokie, IL: Construction Technology Laboratories, Inc, 1988.
9. Donaldson, C. du P. and R. S. Snedeker. "A Study of Free Jet Impingement, Part I--Mean Properties of Free and Impinging Jets." Journal of Fluid Mechanics. (45, Part 2) 1971. 281-319.
10. Fluk, Harold. "High Temperature/Pressure Testing of Heat Resistant Runway Materials." AIAA Aircraft Design, Systems and Technology Meeting. Fort Worth, TX: AIAA, 17-19 Oct. 1983.
11. Fozard, J. W. "Tactical Jet V/STOL - Its Future in a CTOL World." V/STOL/STOVL, SP-680 Aerospace Technology Conference and Exposition. Long Beach, CA: Oct. 1986.
12. Ground Environment Meeting. NAVAIR. Dec. 1988.
13. Harvey, H. M. "Lift Engines: Applied History." Proceedings of the International Powered Lift Conference. Warrendale, PA: Society of Automotive Engineers, Feb. 1988.
14. "Heavy Trucks, Climate and Pavement Damage." Road Transport Research. Paris: OECD, 1988.
15. Higgins, C. C. and T. W. Wainwright. Dynamic Pressure and Thrust Characteristics of Cold Jets Discharging from Several Exhaust Nozzles Designed for VTOL Downwash Suppression. (NASA TN D-2263) Washington, D.C.: NASA, Apr. 1964.
16. Incropera, Frank P. and David P. Dewitt. Fundamentals of Heat Transfer. New York: John Wiley & Sons, 1981.

17. Jenista, John E. and Arthur E. Sheridan. "Configuration E-7 Supersonic STOVL Fighter/Attack Technology Program." Proceedings of the International Powered Lift Conference. Warrendale, PA: Society of Automotive Engineers, Feb. 1988.
18. Kandebo, Stanley W. "Governments, Industry Pool Supersonic STOVL Efforts." Aviation Week & Space Technology. Apr. 11, 1988.
19. Knott, P. G. "The Ground Environment Created by High Specific Thrust Vertical Land Aircraft." Proceedings of the International Powered Lift Conference. Warrendale, PA: Society of Automotive Engineers, Feb. 1988.
20. Koenig, David G. "V/STOL Wind Tunnel Testing." AGARD-R-710 Special Course on V/STOL Aerodynamics. Apr. 1984.
21. Kotansky, Donald R. Investigation of the Interaction of Lift Jets and a Ground Plane. (NASA-CR-152343, NTIS N81-23026) St. Louis, MO: McDonnell Aircraft Co., Apr. 1980.
22. Lewis, W. J. "V/STOL Propulsion System Aerodynamics." AGARD-R-710 Special Course on V/STOL Aerodynamics. Apr. 1984.
23. Lotz, M. and P. Bartels. "Problems of V/STOL Aircraft Connected with the Propulsion System as Experienced on the DO31 Experimental Transport Aircraft." AGARD-CP-135 V/STOL Propulsion Systems. Jan. 1974.
24. Marsell, Michael. "Applying Vectored Thrust V/STOL Experience in Supersonic Designs." Proceedings of the International Powered Lift Conference. Warrendale, PA: Feb. 1988.
25. Mitchell, W., et al. Hot Gas Surface Erosion Studies. (DTIC AD-241 779, ASD-TN60 183) Wright-Patterson AFB, OH: ASD, Aug. 1960.
26. Muir, J. F. Response of Concrete Exposed to a High Heat Flux on One Surface. (NTIS SAND-77-1467) Albuquerque, NM: Sandia Labs, Nov. 1977.
27. National Full-Scale Aerodynamics Complex. NASA Ames Research Center CA: 1987.
28. Popov, E. P. Mechanics of Materials. Englewood Cliffs, NJ: Prentice-Hall, 1972.
29. Purdue University. Thermophysical Properties Research Center. Thermo-physical Properties of Matter. New York: IFI/Plenum, 1970.
30. Ransom, E. C. P. "Introduction and Review of Jet Interference Phenomena Relevant to V/STOL Aircraft." AGARD-R-710 Special Course on V/STOL Aerodynamics. Apr. 1984.
31. Reynolds, William C. and Henry C. Perkins. Engineering Thermodynamics. McGraw Hill, Inc. 1977.
32. Shapiro, Ascher H. The Dynamics and Thermodynamics of Compressible Fluid Flow. New York: Ronald Press, 1953.
33. Smith, Peter. "Resistance to High Temperatures." Significance of Tests and Properties of Concrete and Concrete - Making Materials. (ASTM Special Technical Publication 169B) Philadelphia, PA: American Society for Testing and Materials, 1978.

34. United Technologies, Pratt & Whitney Aircraft.
Aeronautical Vest-pocket Handbook. Aug. 1981.
35. Van Dalsem, W. R., A. G. Panaras and J. L. Steger.
"Numerical Investigation of a Jet in Ground Effect with a
Crossflow." Proceedings of the International Powered Lift
Conference. Warrendale, PA: Society of Automotive
Engineers, Feb. 1988.

APPENDIX A
MATERIAL TEMPERATURE PROFILES

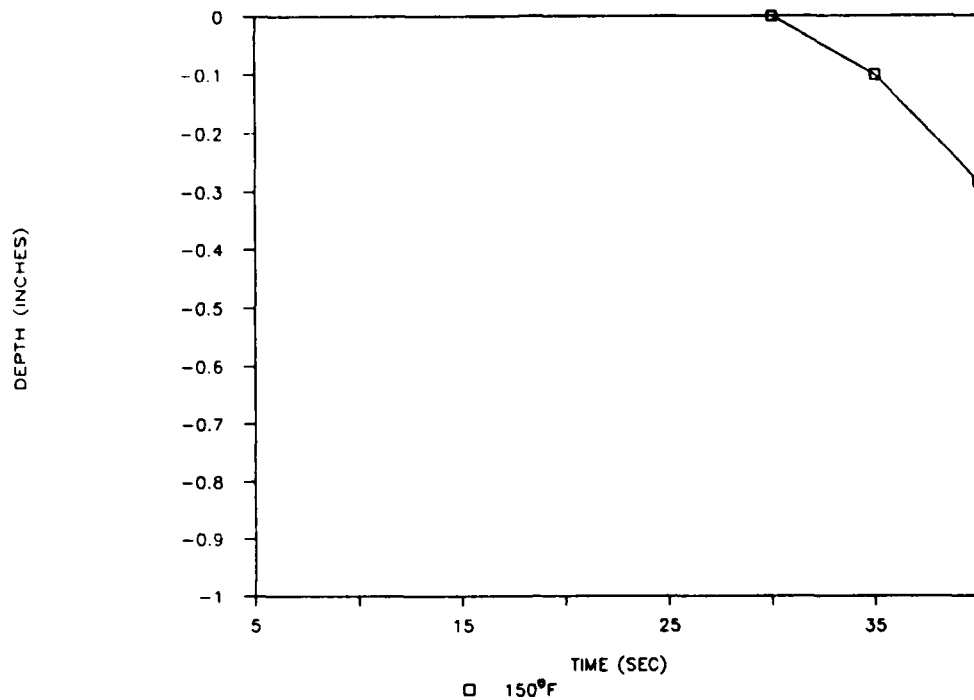


Figure A-1. Temperature Profile in Aluminum (10 Btu/ft²-sec)

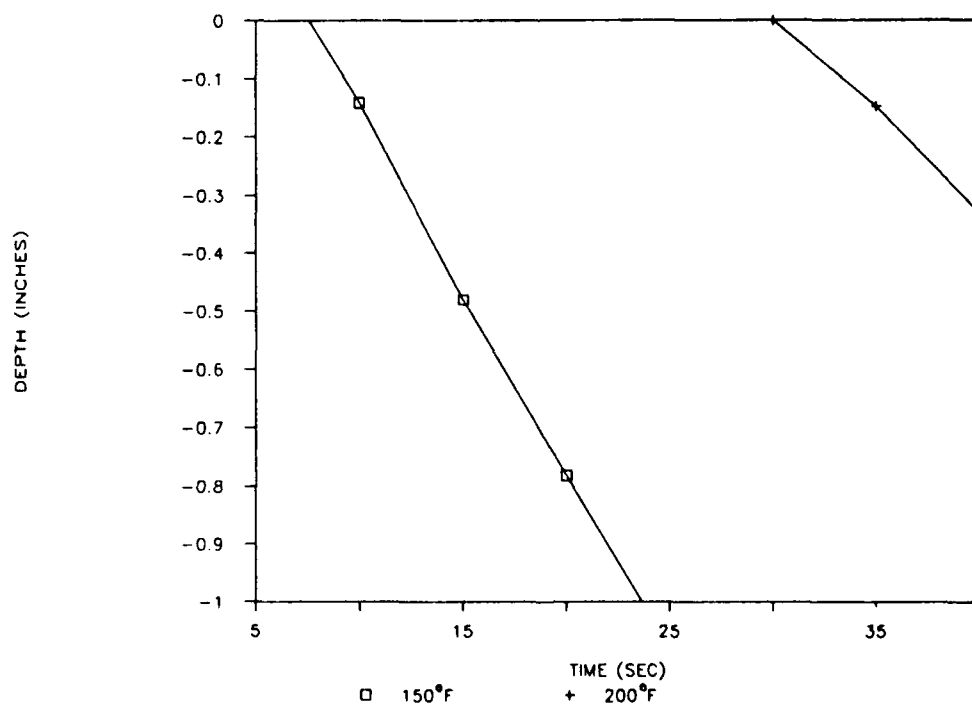


Figure A-2. Temperature Profile in Aluminum (20 Btu/ft²-sec)

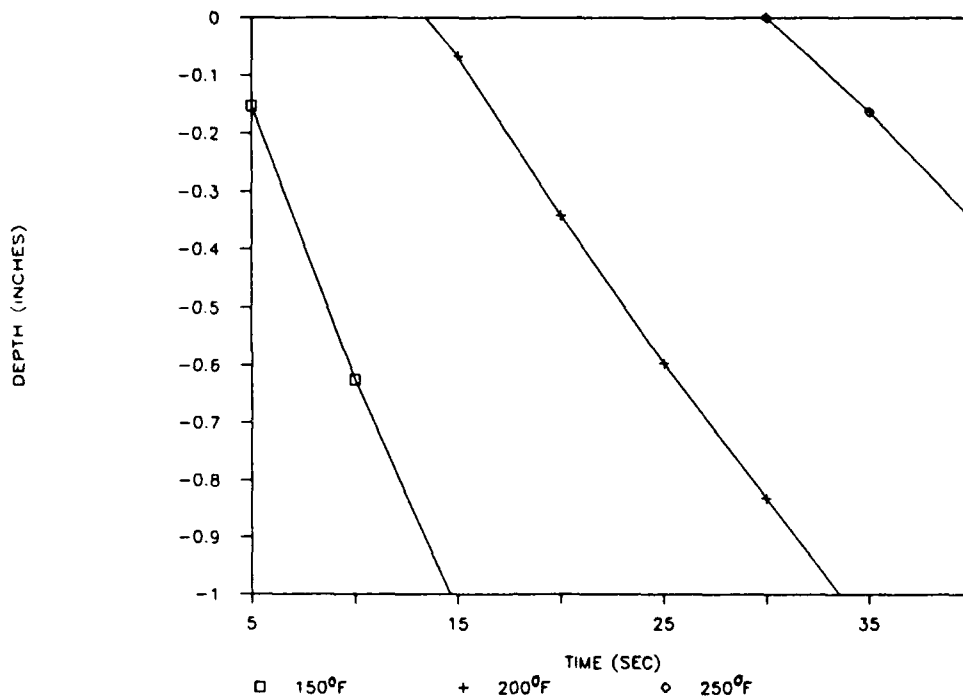


Figure A-3. Temperature Profile in Aluminum (30 Btu/ft²-sec)

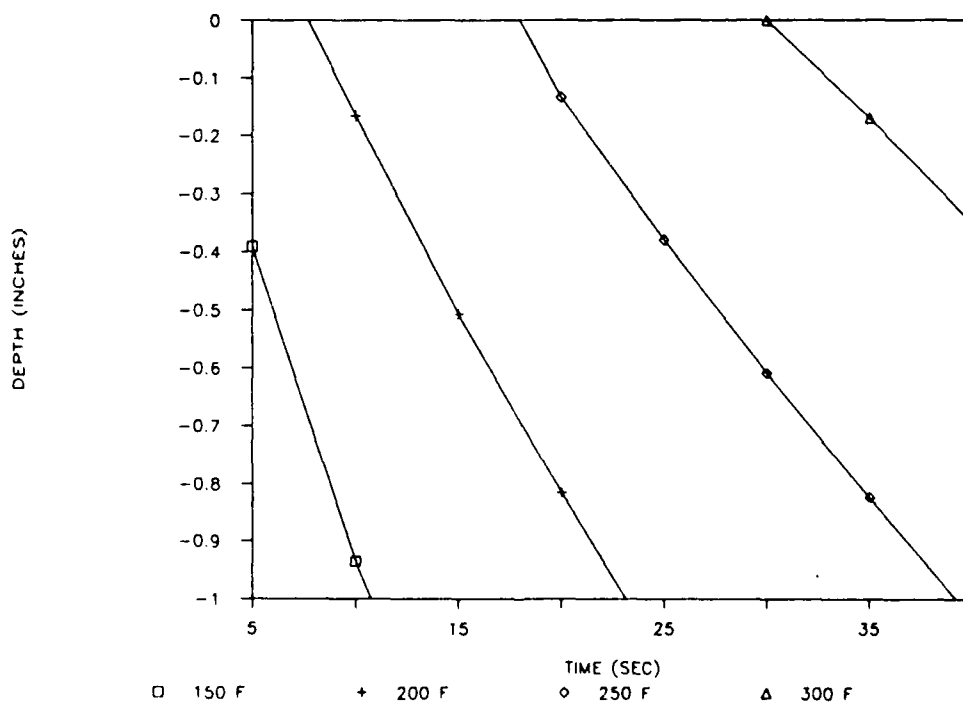


Figure A-4. Temperature Profile in Aluminum (40 Btu/ft²-sec)

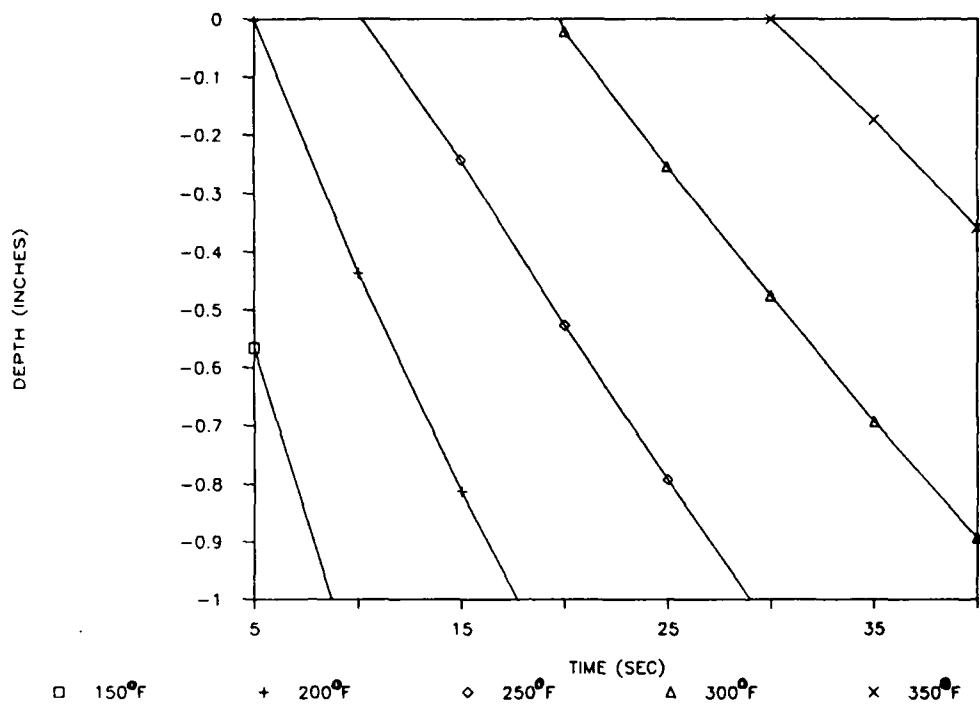


Figure A-5. Temperature Profile in Aluminum (50 Btu/ft²-sec)

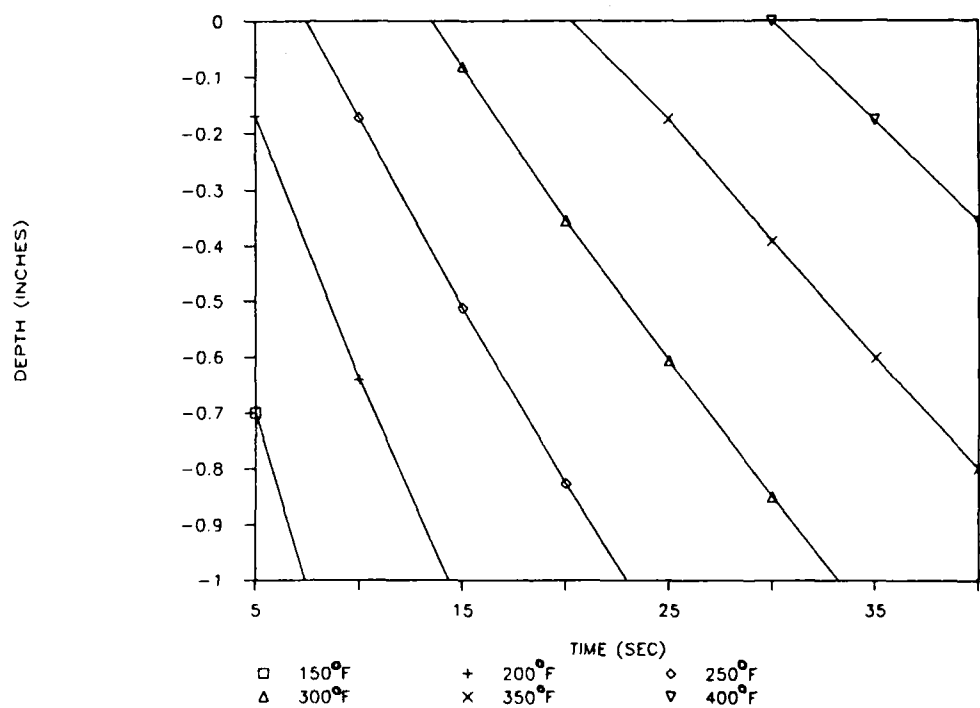


Figure A-6. Temperature Profile in Aluminum (60 Btu/ft²-sec)

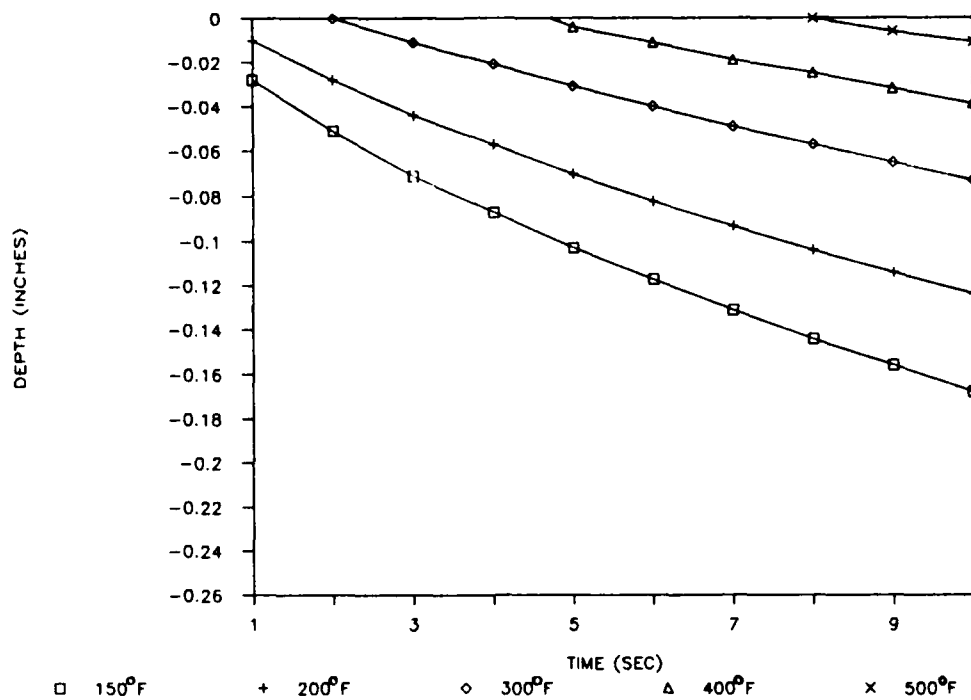


Figure A-7. Temperature Profile in Asphalt (10 Btu/ft²-sec)

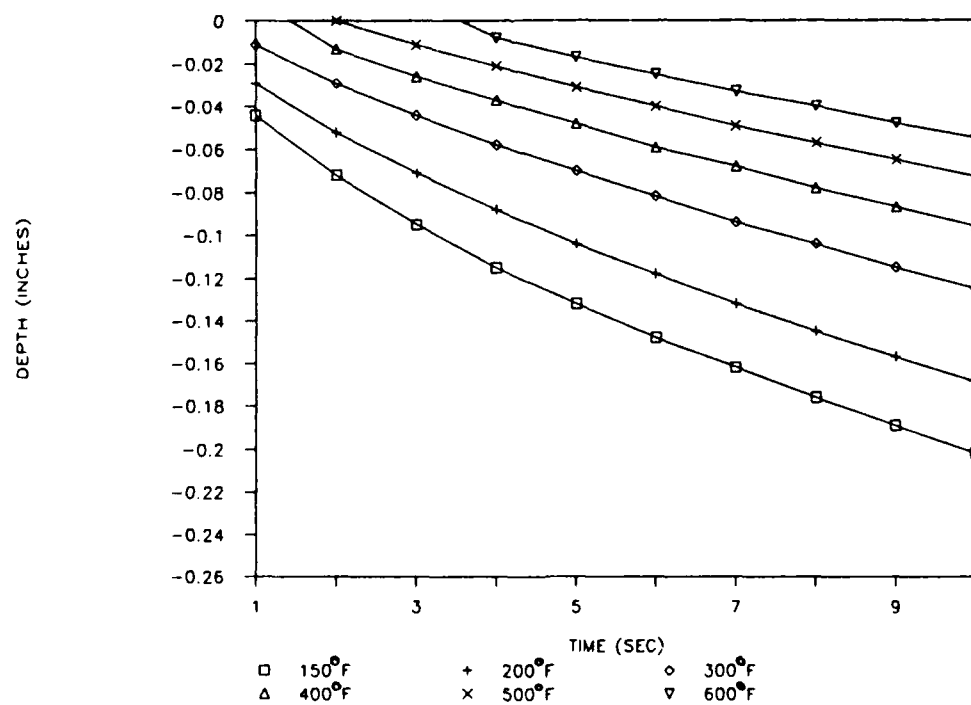


Figure A-8. Temperature Profile in Asphalt (20 Btu/ft²-sec)

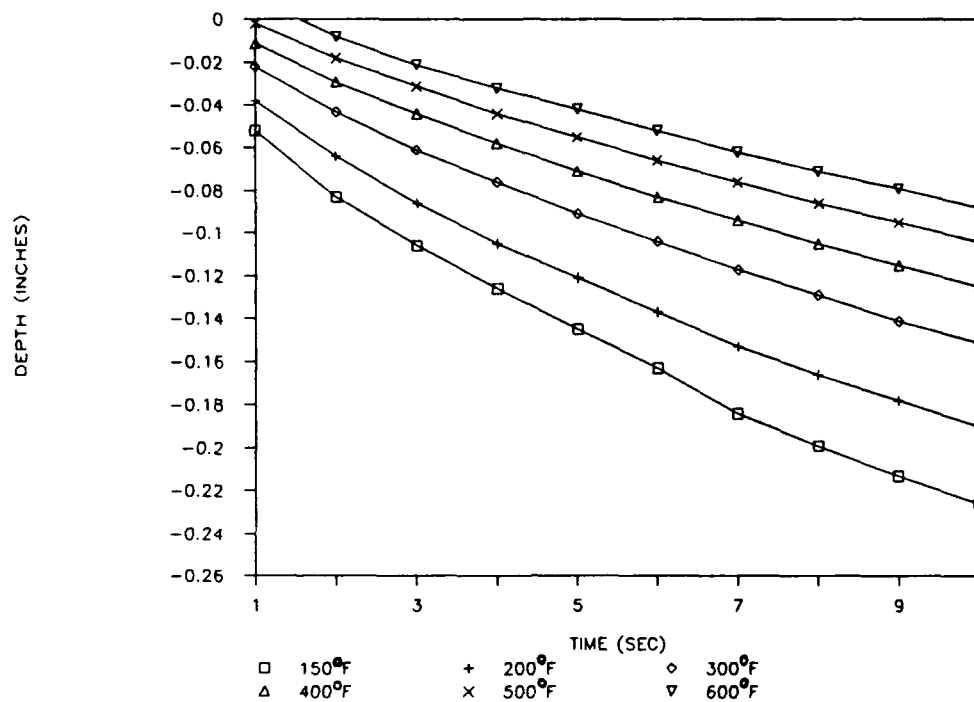


Figure A-9. Temperature Profile in Asphalt (30 Btu/ft²-sec)

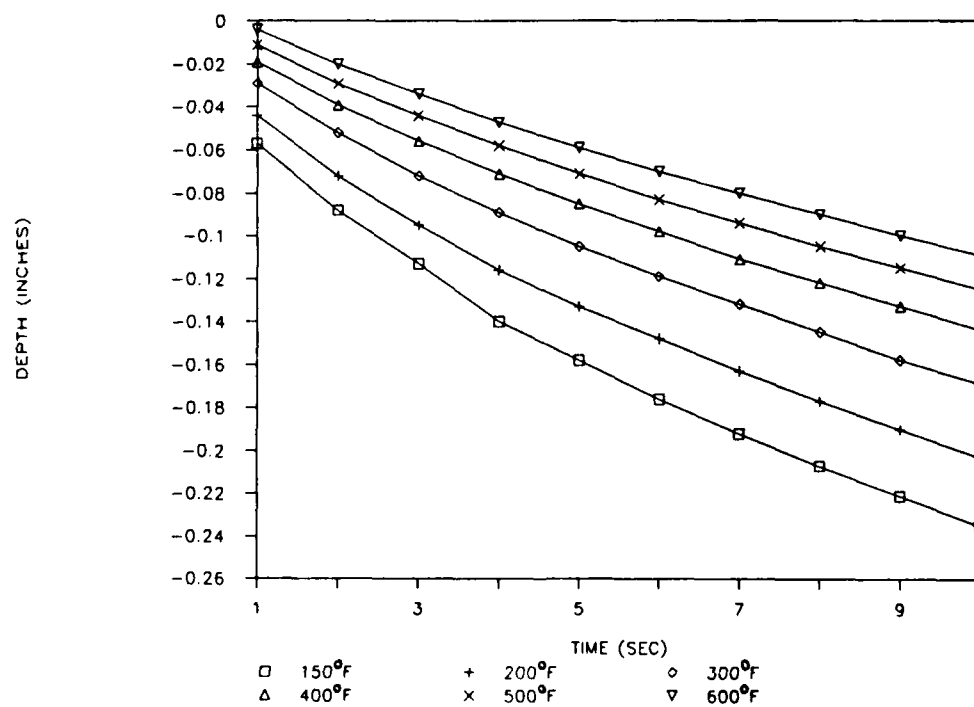


Figure A-10. Temperature Profile in Asphalt (40 Btu/ft²-sec)

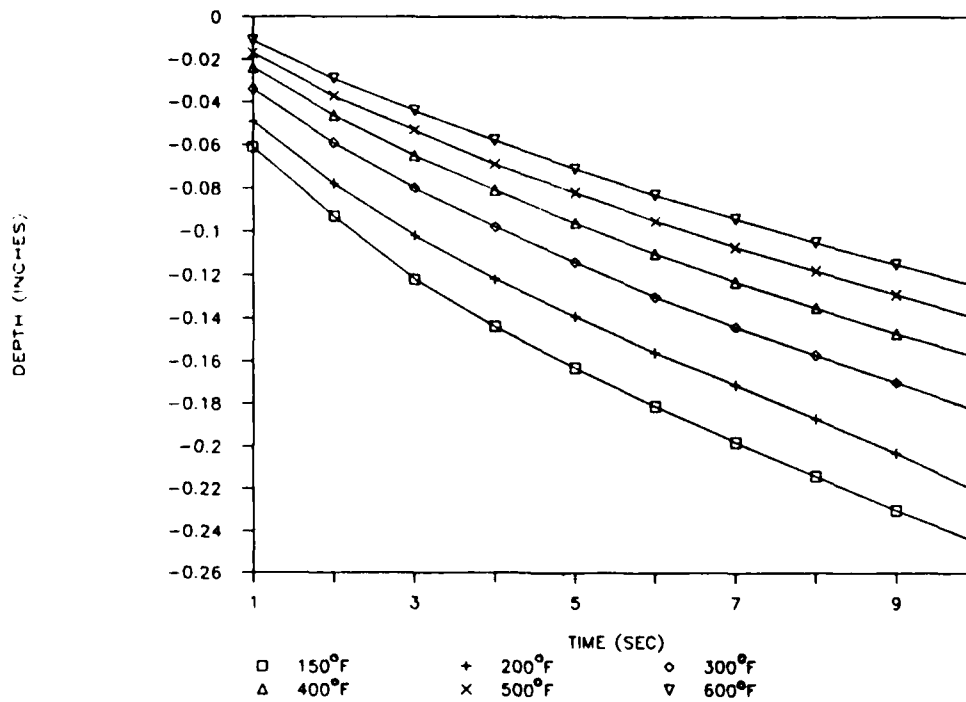


Figure A-11. Temperature Profile in Asphalt (50 Btu/ft²-sec)

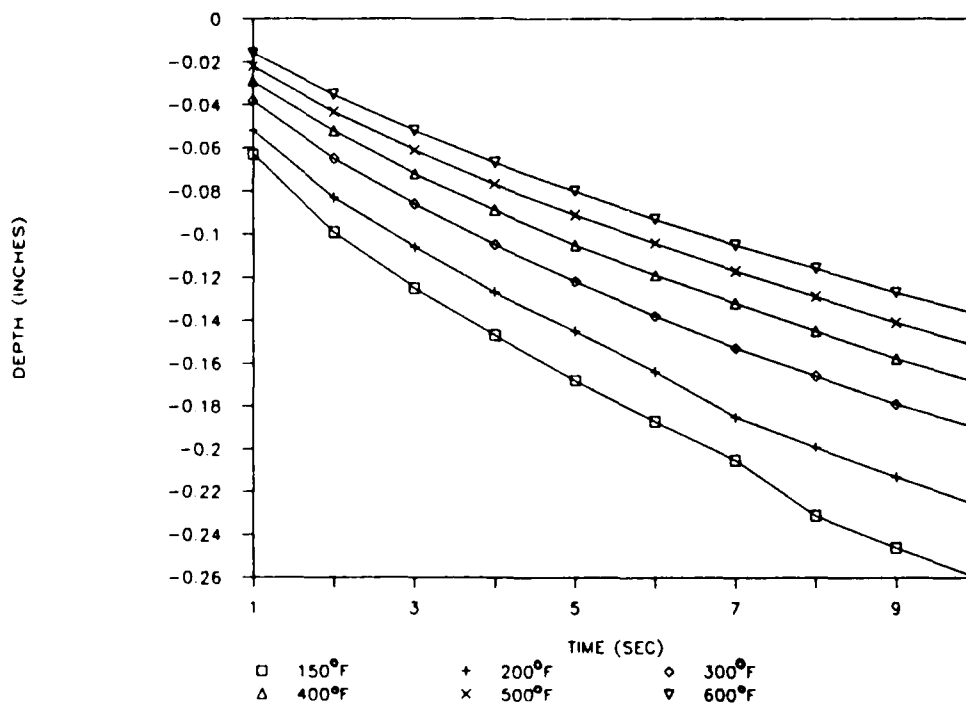


Figure A-12. Temperature Profile in Asphalt (60 Btu/ft²-sec)

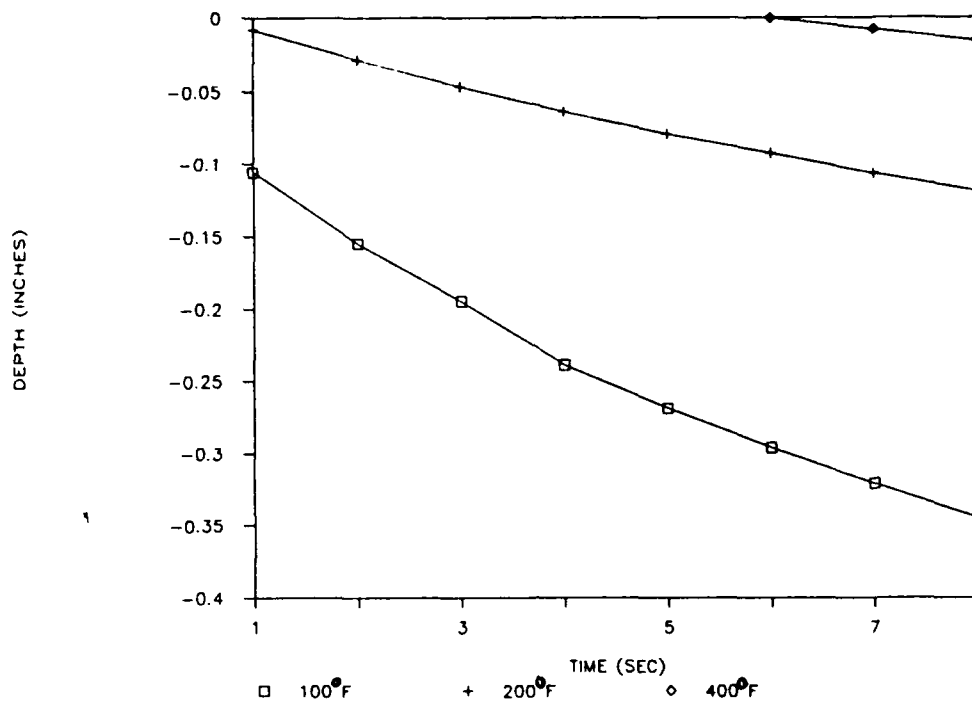


Figure A-13. Temperature Profile in PCC (10 Btu/ft²-sec)

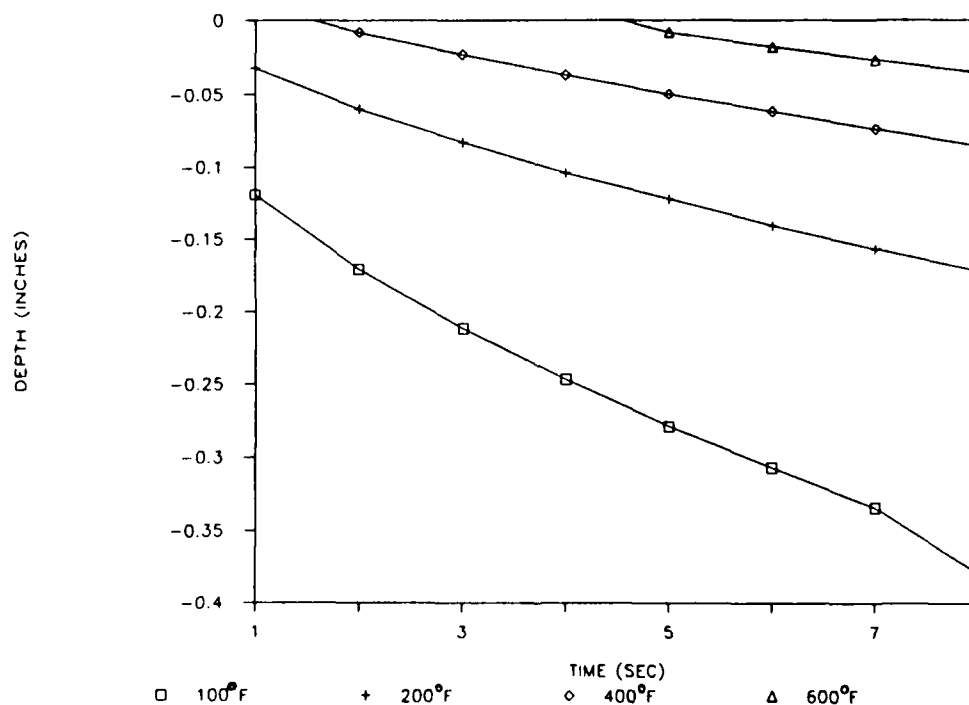


Figure A-14. Temperature Profile in PCC (20 Btu/ft²-sec)

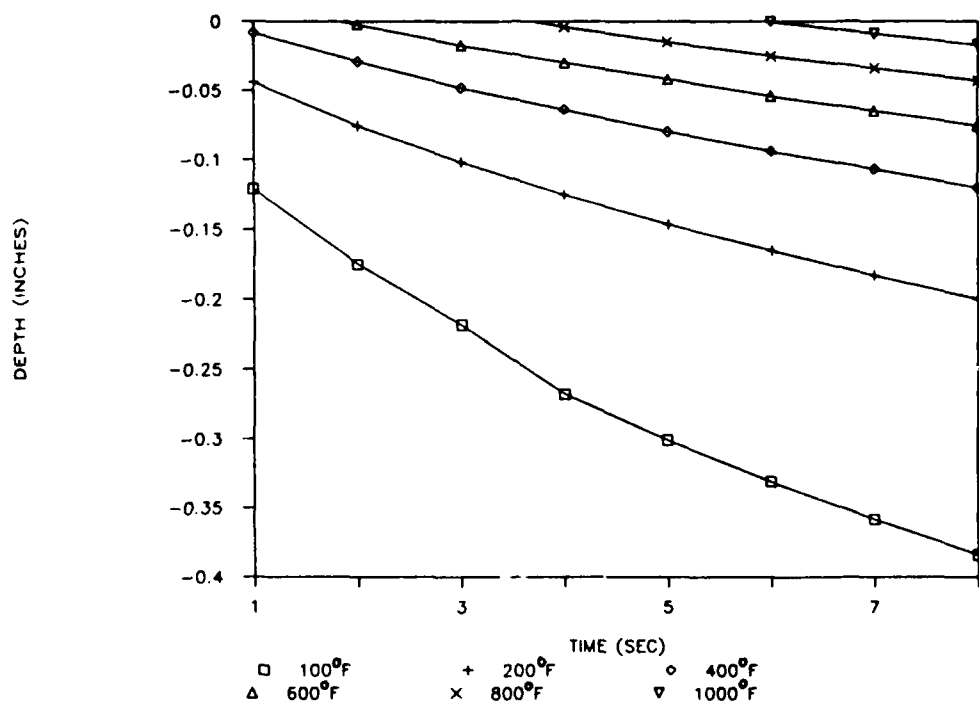


Figure A-15. Temperature Profile in PCC (30 BTU/ft²-sec)

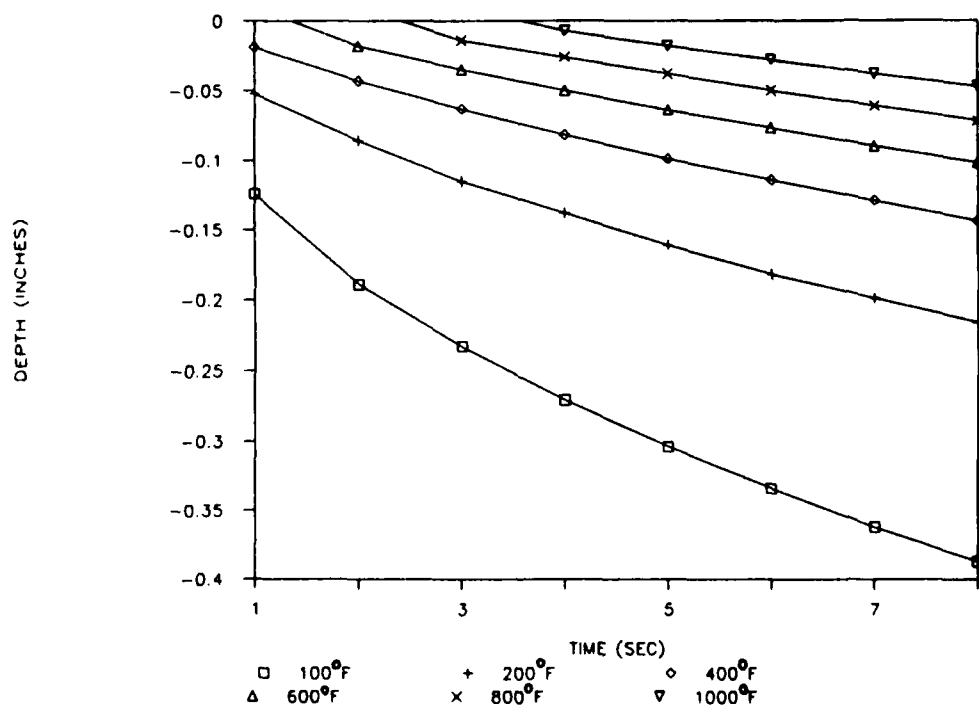


Figure A-16. Temperature Profile in PCC (40 Btu/ft²-sec)

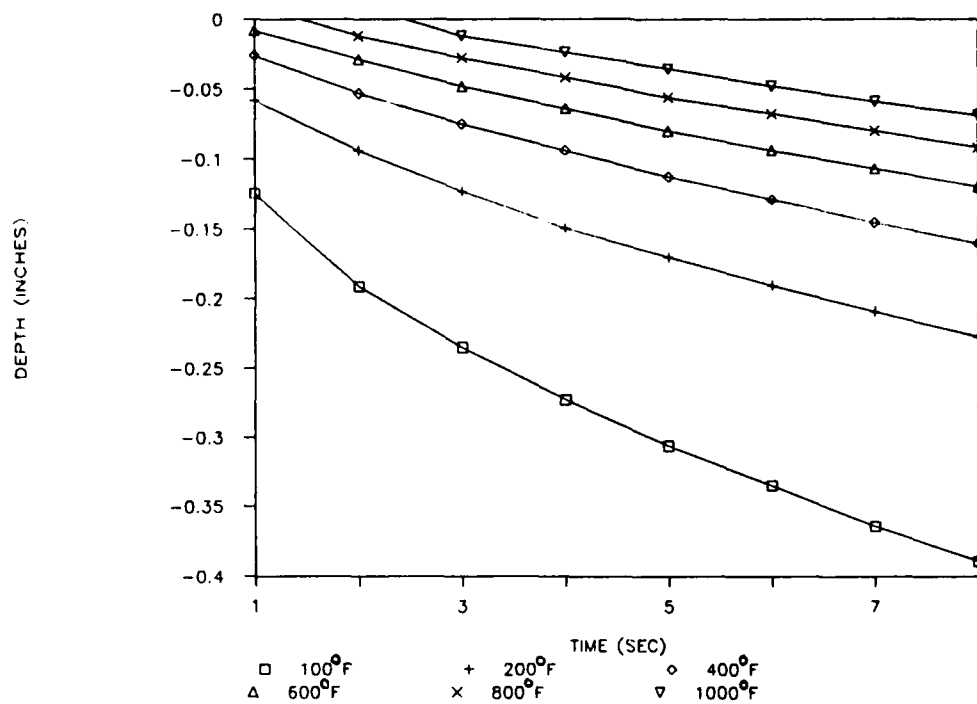


Figure A-17. Temperature Profile in PCC (50 Btu/ft²-sec)

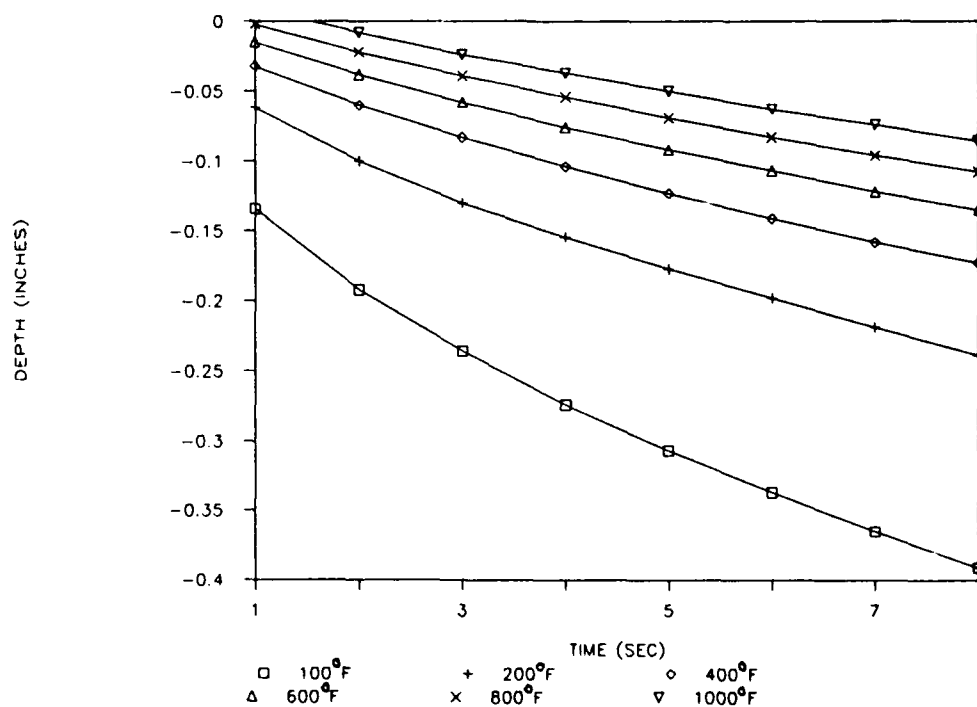


Figure A-18. Temperature Profile in PCC (60 Btu/ft²-sec)

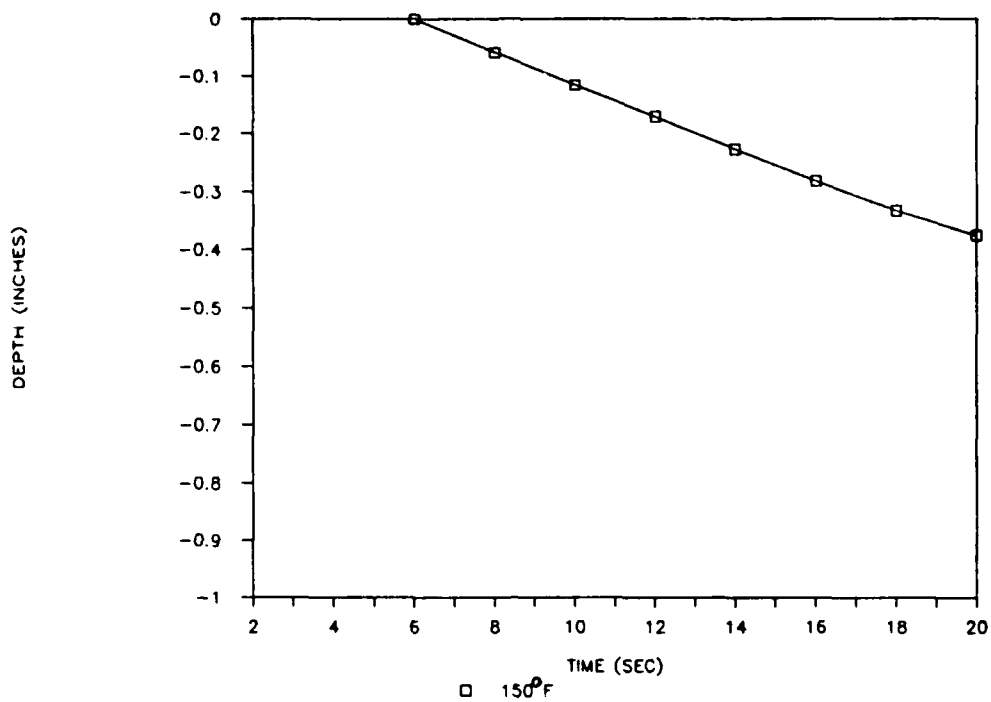


Figure A-19. Temperature Profile in Steel (10 Btu/ft²-sec)

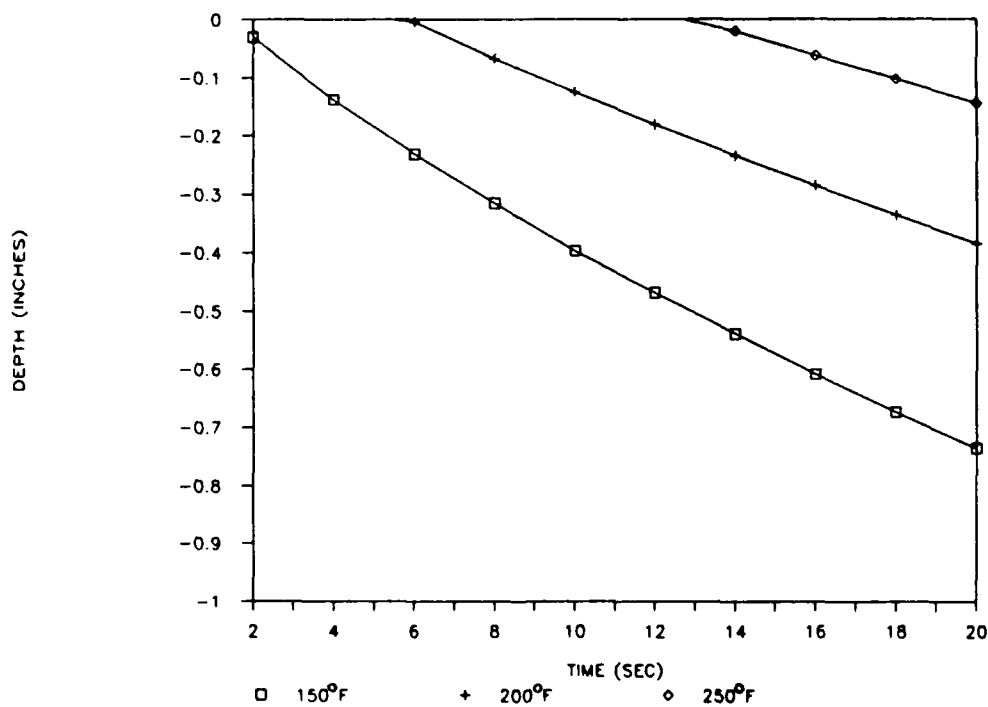


Figure A-20. Temperature Profile in Steel (20 Btu/ft²-sec)

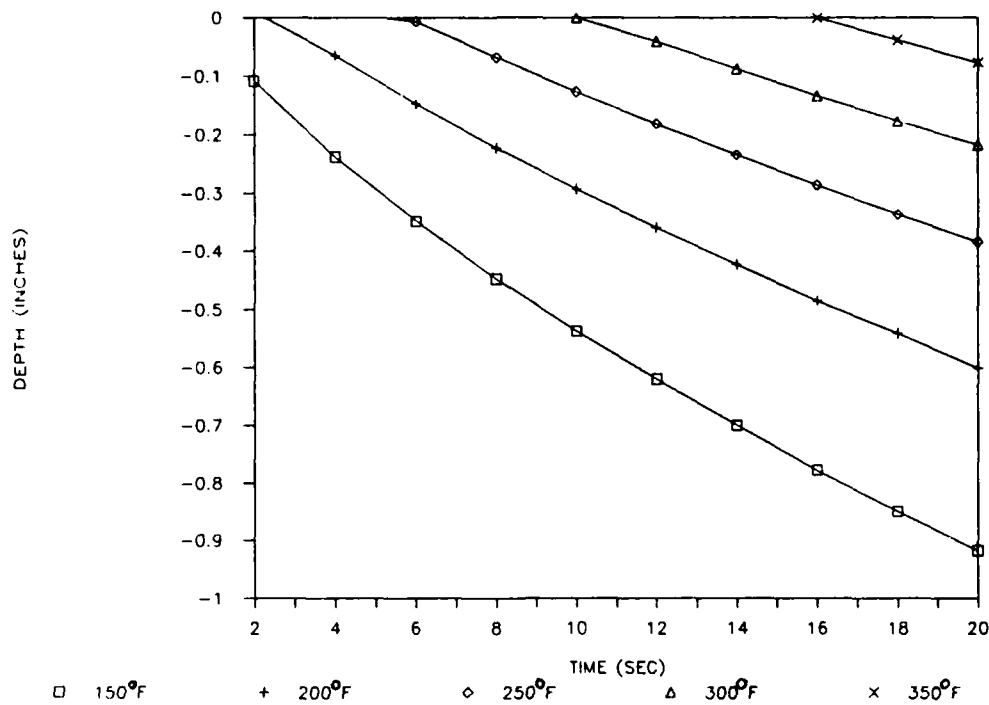


Figure A-21. Temperature Profile in Steel (30 Btu/ft²-sec)

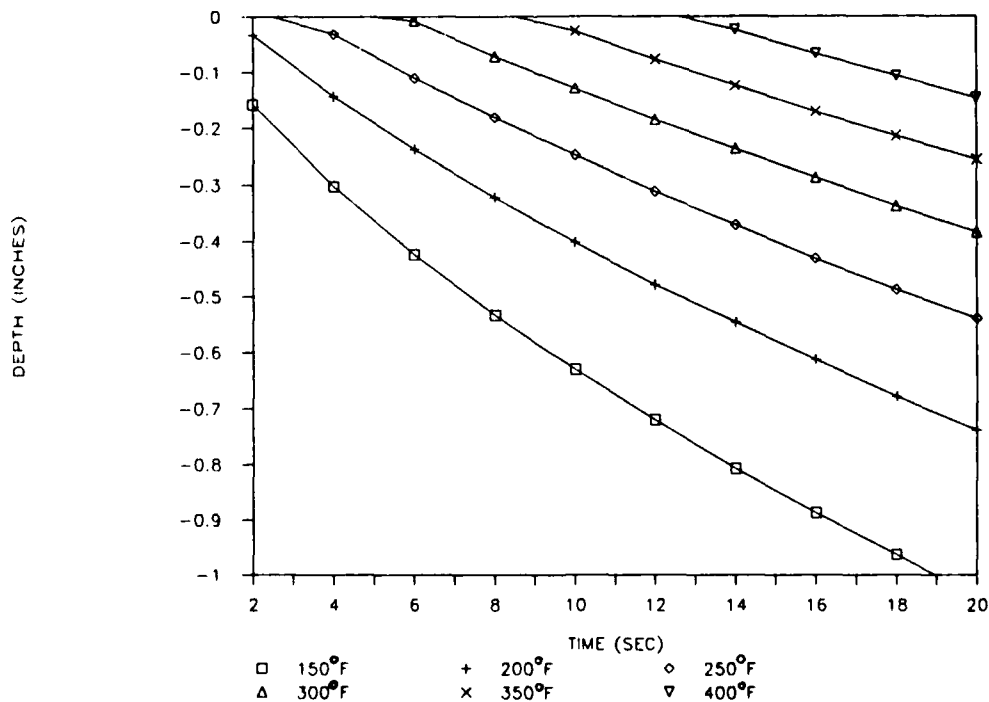


Figure A-22. Temperature Profile in Steel (40 Btu/ft²-sec)

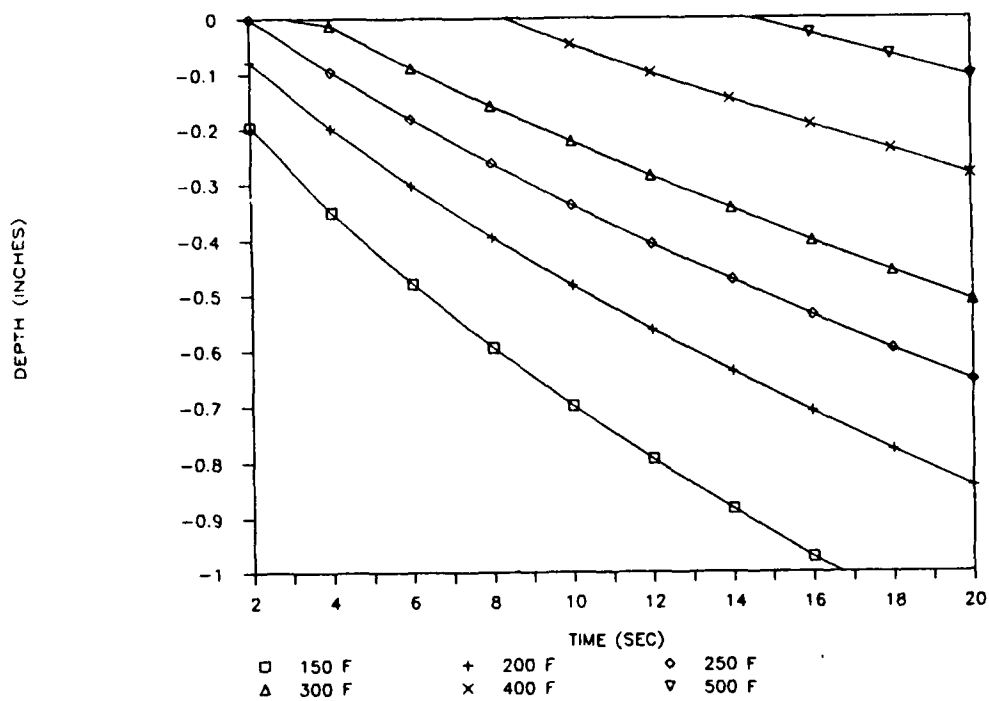


Figure A-23. Temperature Profile in Steel (50 Btu/ft²-sec)

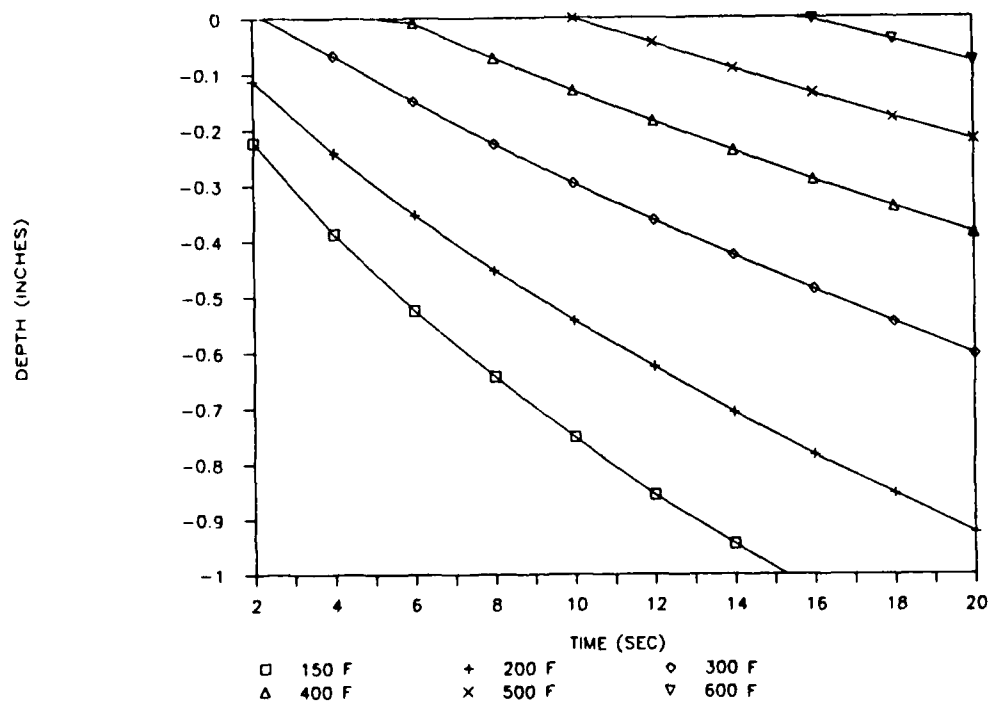


Figure A-24. Temperature Profile in Steel (60 Btu/ft²-sec)

APPENDIX B
TEST FACILITIES

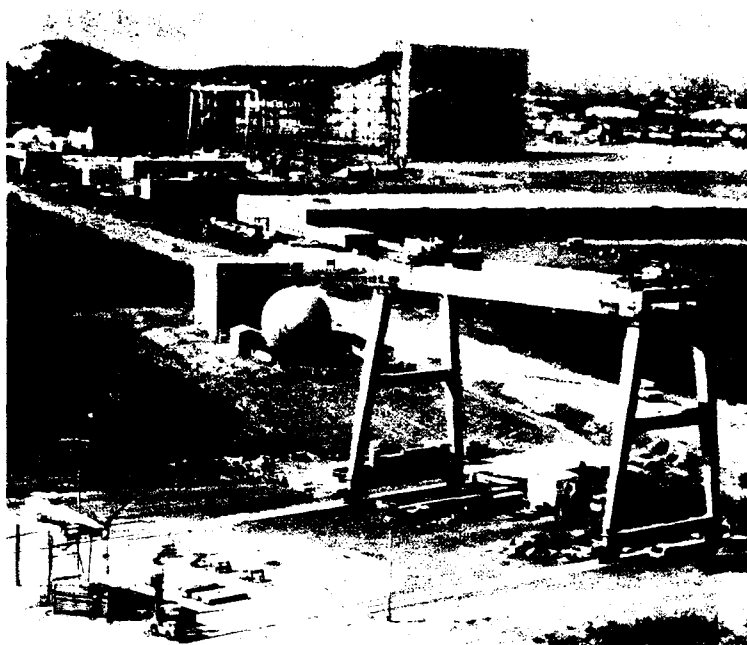


Figure B-1. NASA Ames Outdoor Aerodynamic Research Facility²⁷

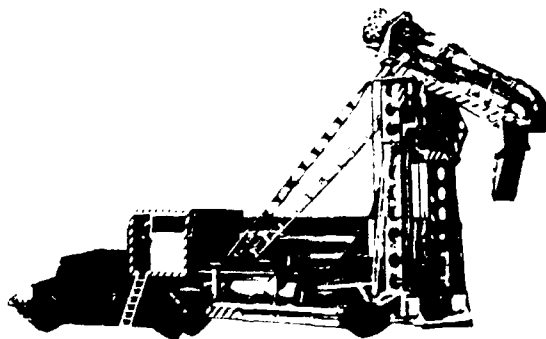


Figure B-2. Moveable Ground Erosion Rig²³

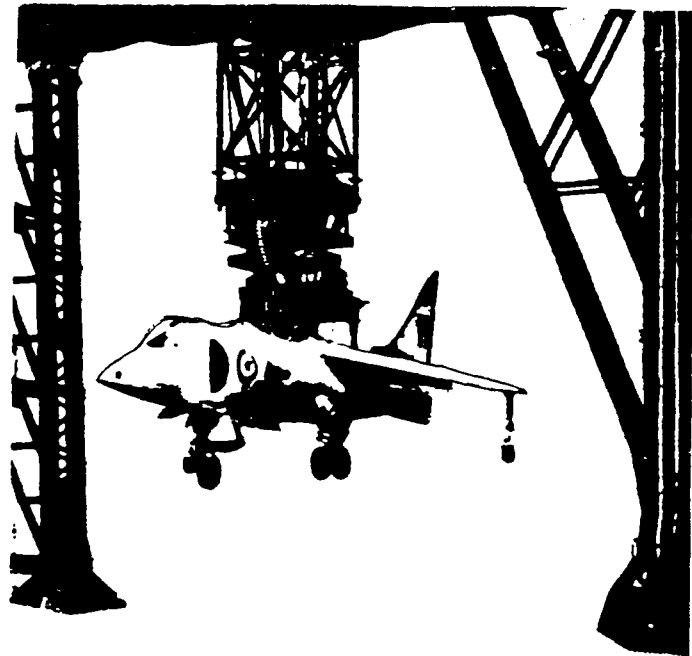


Figure B-3. ShoeBuryness Test Site¹¹

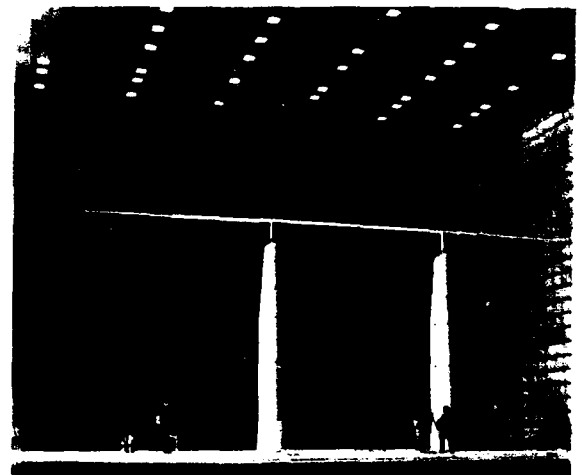
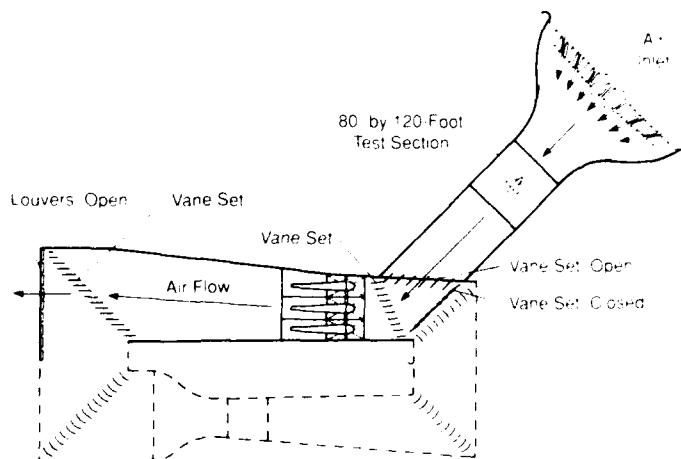


Figure B-4. NASA Ames 80 X 120 Wind Tunnel²⁷

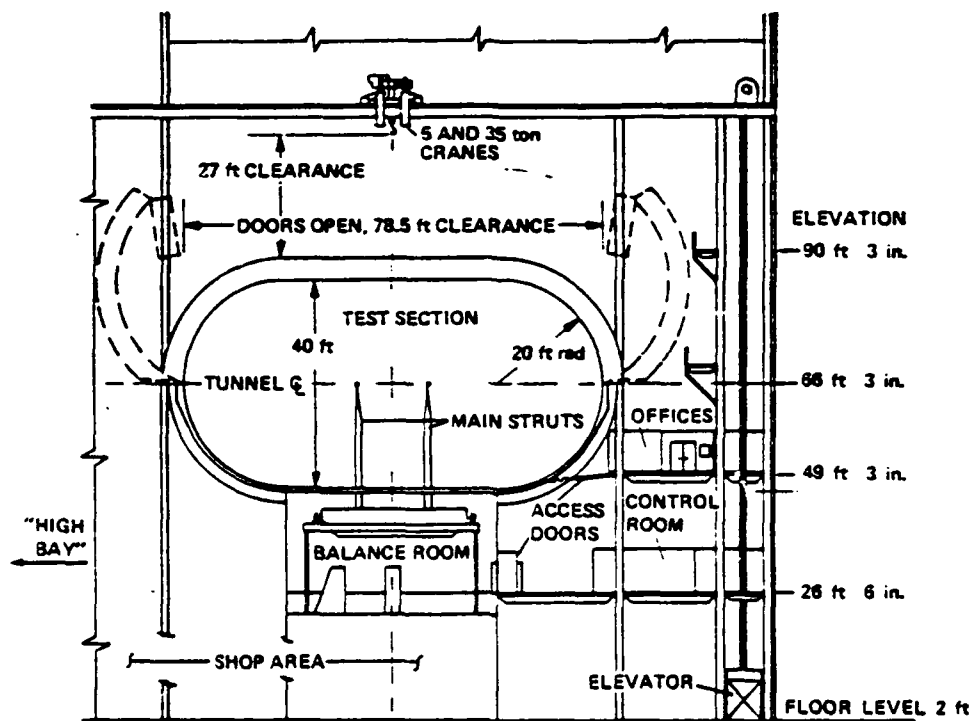


Figure B-5. NASA Ames 40 X 80 Wind Tunnel²⁰

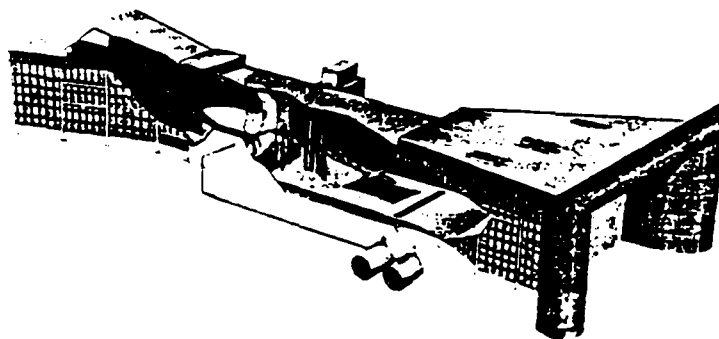
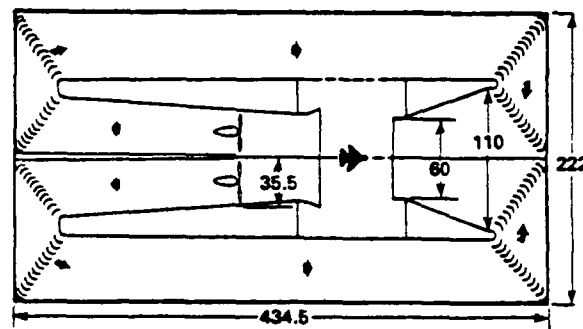


Figure B-6. British Aircraft Corporation 5.5 Meter Wind Tunnel³⁰



ALL DIMENSIONS IN FEET

Figure B-7. NASA Langley 30 X 60 Wind Tunnel²⁰

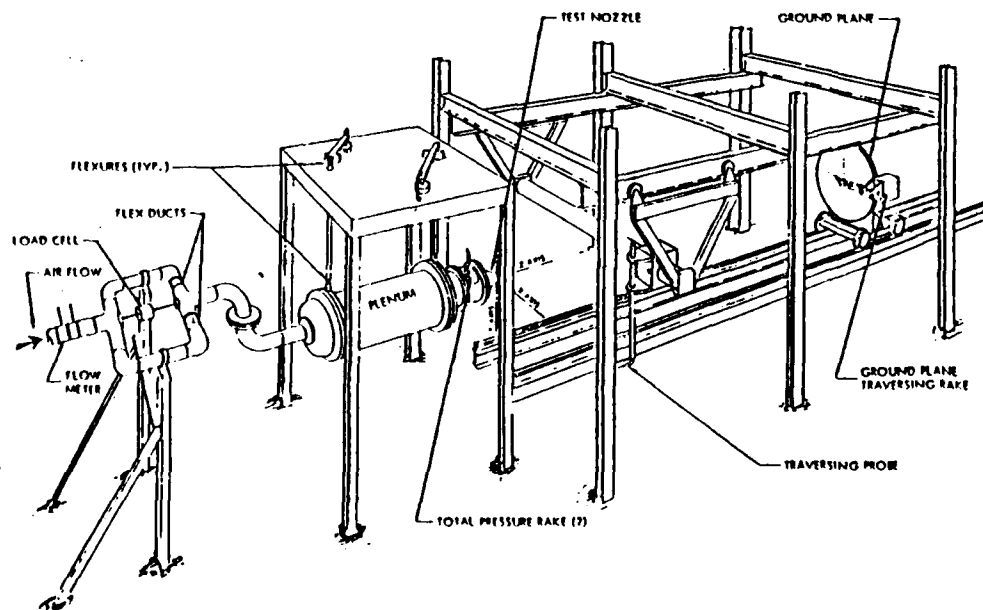


Figure B-8. Boeing Cold Air Rig¹⁵

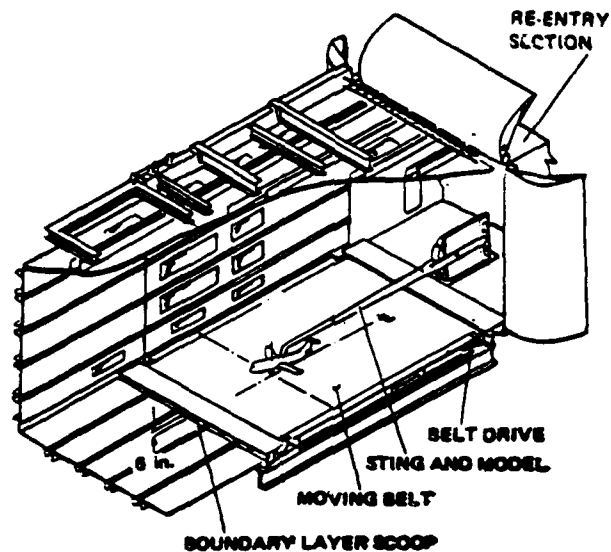


Figure B-9. Boeing V/STOVL Wind Tunnel²⁰

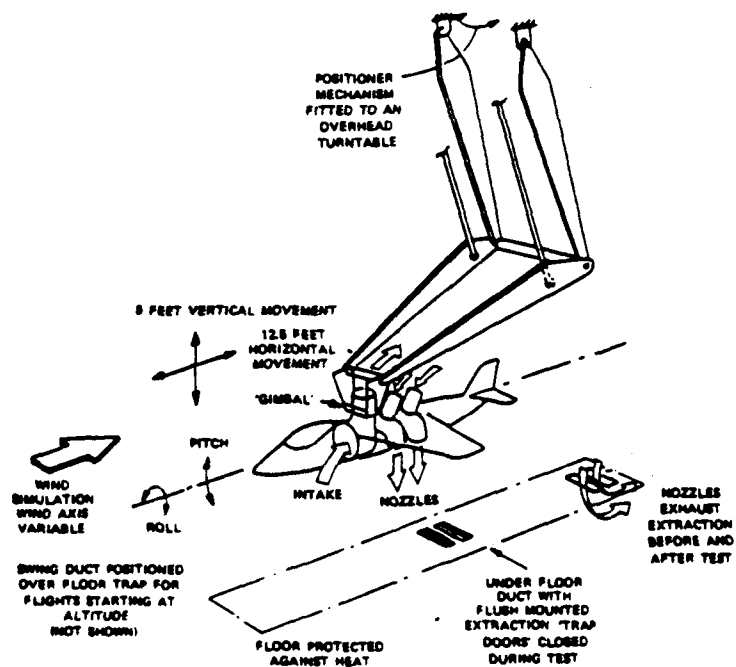


Figure B-10. British Aerospace Hot Gas Ingestion Facility⁵

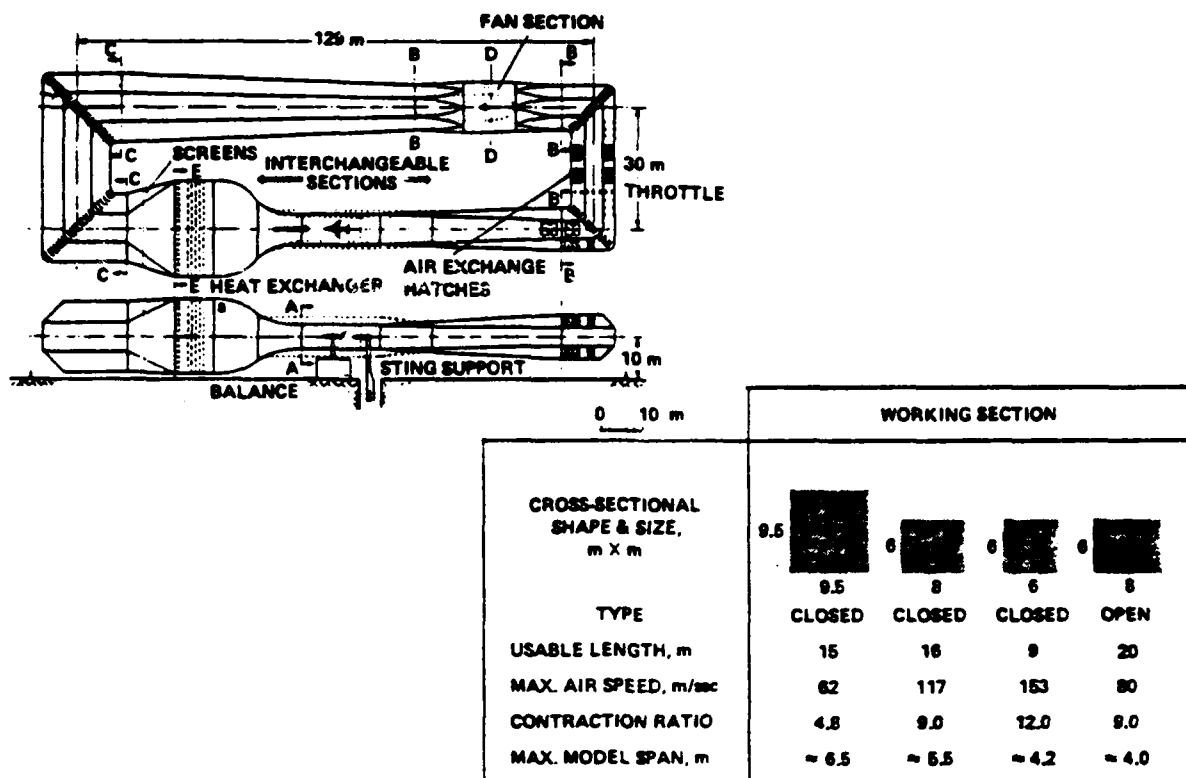


Figure B-11. German/Dutch Low Speed Wind Tunnel DWN²⁰

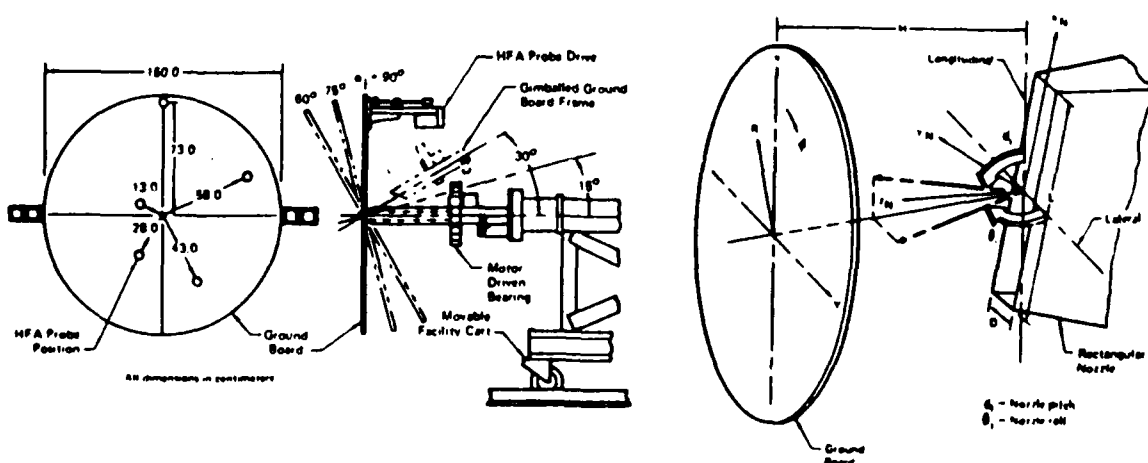


Figure B-12. McDonnell Aircraft Jet Interaction Test Apparatus²¹

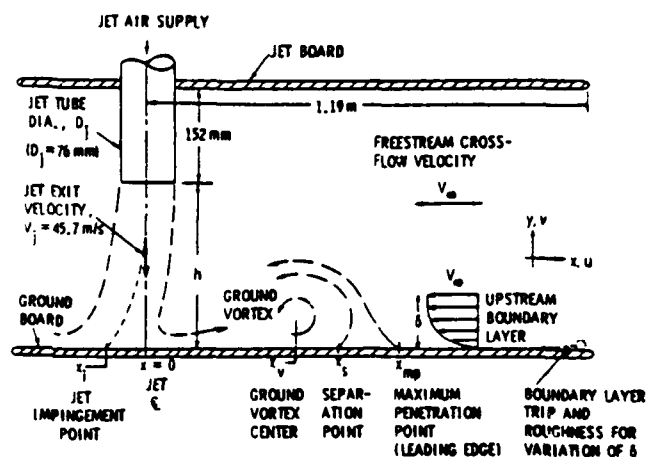
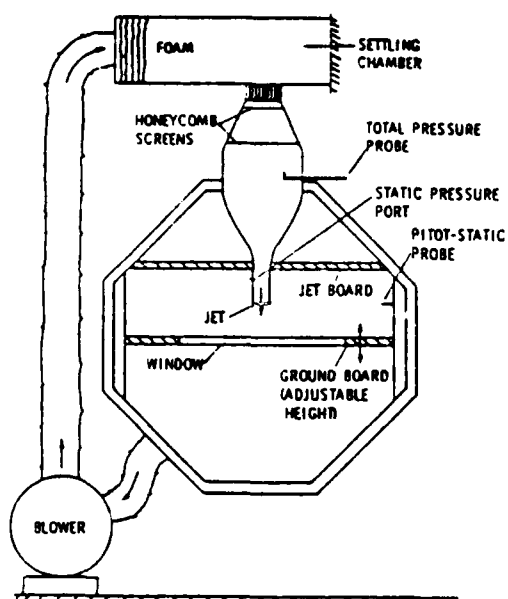


Figure B-13. Pennsylvania State University Laboratory⁷

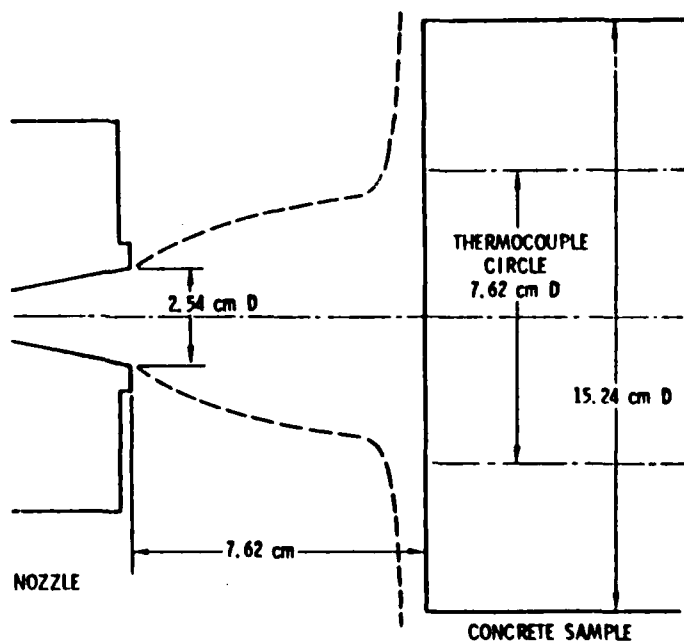
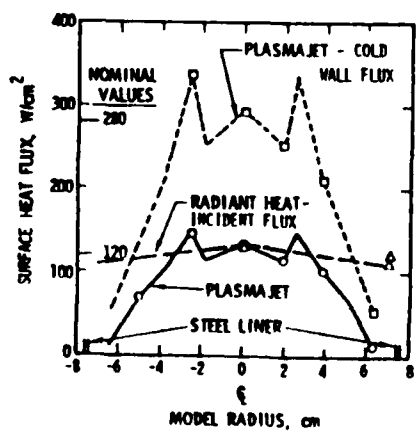
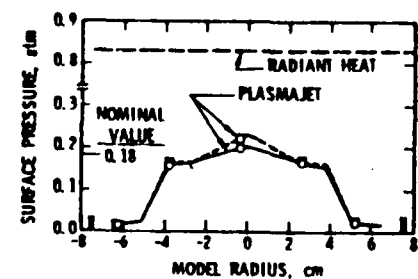


Figure B-14. Sandia Laboratory²⁶